Modeling a four-wave mixing scheme for trapped-atom qubit measurement

by

Marissa McMaster

Committee in charge:

Associate Professor in Physics Minhyea Lee, Thesis Advisor
Professor Adjoint in Physics Jun Ye, Honors Council Representative
Assistant Professor in Mathematics Robin Deeley, Outside Reader

Department of Physics
University of Colorado at Boulder
Defended April 10, 2023

Abstract

At the moment, one of the most popular approaches to trapped-atom qubit measurement is measurement by resonance fluorescence, which, while relatively easy to implement, is susceptible to yielding noisy results because the measurement signal and the field used to initiate the measurement have the same frequency. A proposed alternative to this measurement scheme is that performed by a four-wave mixing (FWM) process, which would permit the measurement signal to have a frequency distinct from those used to initiate the measurement, allowing for the measurement signal to be easily filtered from other frequencies in the system and reducing measurement noise. This thesis seeks to model FWM stimulated in a trapped-atom system, then to derive from the model an expression for the efficiency of the process. To do this, we solve the wave equation of the signal field generated by FWM analytically before using Python to offer a numerical solution to the problem. The result is a set of Python scripts which can calculate the FWM efficiency and the optical power of the generated signal as a function of various system parameters, but making a conclusion on the viability of a FWM-based measurement scheme would likely involve a sophisticated optimization algorithm and knowledge of specific hardware limitations.

to Grandma Ruth: this is the culmination of the greatest gift you've ever given me. I'm more appreciative of it than you will ever know.

Acknowledgements

This thesis would not have been possible without the help of many people, but it certainly would have been extra-challenging without the guidance of Eric Copenhaver and Alex Radnaev. The day I met Eric, I almost passed out in the lab because I had just gotten my wisdom teeth taken out and I wasn't eating anything. I remember him asking if I wanted a bagel. Ever since then, Eric has been extremely committed to helping me out, to an extent that is inspiring and something I want to mimic as my career advances. I am extremely grateful that Eric spent multiple hours each week for the past ten months talking with me about physics, helping me troubleshoot my code, and patiently listening to me while I had multiple crises that made me question my understanding of even the most simple quantum mechanical concepts. (Here's to hoping that I can finally memorize what quantum numbers are.) All jokes aside, thank you so much for embarking with me on this journey though nonlinear optics, atomic physics, and numerical methods. I feel like I've become a much better physicist with your help, and I'm not sure how to fully describe my gratitude.

This project would quite literally be impossible without the help of Alex Radnaev, who proposed and introduced the topic to me and whose opinion partially encouraged me to write an honors thesis to begin with. It would have also been *figuratively* impossible without his help as I'm not confident that I would have ended up in AMO if he hadn't taken a chance on me by inviting me to work at NIST three and a half years ago when I knew *nothing* about physics and then a second time when he invited me to work at Infleqtion a year later when I knew marginally more about physics. Alex taught me how to *do* physics and *think* like a physicist, all while pushing me to improve and fostering my love for AMO, and for all of this, I feel indebted to him in some way. I'm unbelievably grateful for every opportunity he's given me and all the advice, encouragement, and help he's provided over the years. Thanks for showing me that I can have a career in physics.

I'd like to extend my greatest thanks to Professor Minhyea Lee, who saw something in me even after I failed spectacularly to make a functioning AM radio in J-lab. Prof. Lee encouraged me to write this thesis and provided uncountable amounts of well-needed affirmations that I was doing well in school and in physics more generally. I am so thankful

that she continually agreed to meet with me just to chat about how things were going and to answer my silly questions. I'm not sure I could have made it through my junior and senior years without a professor to talk to who clearly cared about me and appreciated what I could do; Prof. Lee's support made a huge difference for me.

Thanks also to Professors Jun Ye and Robin Deeley, who made time in their busy schedules to serve on my committee. Special thanks to Prof. Deeley, who agreed to serve on the committee on such short notice after my earlier plans fell through; it was getting to a point where I thought I wouldn't be able to hold a thesis defense.

I probably would have dropped out of physics without the academic and moral support of three very special people: Will, Brooke and Dion, who have all spent way too much time, most of it concentrated on Friday nights, working through math and physics problem sets with me. Over the past three and a half years, we've experienced nearly every emotion together, and knowing that I wasn't alone in any of it encouraged me to continue to put in the effort and learn, even when that was the last thing I wanted to do. Just now I racked my brain trying to think of a "should we make the dog bark?" joke to end this on a cute and quirky note, but I couldn't think of a good one. Sorry. I feel very lucky to have been supported by you.

My final round of thanks goes to my family, who each played a distinct role in helping me get this far. Thanks to my mom, Tracy, for sitting on the phone with me for extended periods of time as I ranted or rambled on about nothing or cried about whichever bad grade I got or how I was worried that I wasn't doing enough. Thanks to my grandma, Ruth, for making me smile and always being excited to hear about what I was doing at school or in the lab. I'm so honored that every time you see an article about quantum computing, you think of me. A last special thanks to my dad, Scott, who encouraged my love for the sciences growing up by showing me NOVA documentaries, ~~debugging~~ writing my computer science IAs, and building circuits with me, among many other things. I'm not sure that I would have become a scientist if it wasn't for your encouragement.

Thanks again, everyone, it means the world to me.

Contents

Nomenclature

Γ_2	Decay rate of state 2
Γ_3	Decay rate of state 3
Γ_4	Decay rate of state 4
Ω_p	Rabi frequency of the $1 > 2$ transition
Ω_c	Rabi frequency of the $2 > 3$ transition
Ω_d	Rabi frequency of the $4 > 3$ transition
ω_p	Frequency of the pump beam
ω_c	Frequency of the coupling beam
ω_d	Frequency of the drive beam
Δ_p	Detuning of the pump beam
Δ_c	Detuning of the coupling beam
Δ_d	Detuning of the drive beam

Chapter 1

Introduction

Quantum computers have the potential to expand our knowledge in unimaginable ways and to improve our daily lives by advancing fields such as drug development, cryptography, and solving optimization problems. The development of the trapped-atom and trapped-ion approach to quantum information systems has accelerated in recent years as many groups in both academia and industry attempt to construct one of the first quantum computers with either atomic or ionic qubits with the hopes of unlocking this potential. The specifics of these systems can vary broadly, but they are fundamentally very similar. Each has a chosen atom or ion, in which two orthogonal (often electronic) states are specified to be the $|0\rangle$ and $|1\rangle$ states, together called the "qubit states". Then, computations are performed on the qubits by a set of various frequencies which work to trap them, prepare them into their initial states, entangle them with each other, and apply quantum logic gates, all before ending the process by measuring the final state of the qubit. (Since this paper focuses on trapped-atom qubits, we will stop mentioning trapped-ion qubits, although many of our comments and results will be applicable to them.)

Unfortunately, there remain many improvements to make to any existing trapped-atom computer before it functions entirely as desired. An area in which there is much room for improvement in the development of these systems is that of qubit measurement. One of the most popular approaches to measurement of trapped-atom qubits is called *measurement by resonance fluorescence*.

One of the primary issues with this process is that the frequency emitted by the measured qubit is already present in the system. In other words, when resonance fluorescence is used, the emitted measurement photons and the light used to stimulate the measurement process have the same frequency, which introduces a source of noise if the device used to collect the signal were to measure additional photons that are not a product of spontaneous emission but rather are present for other reasons.

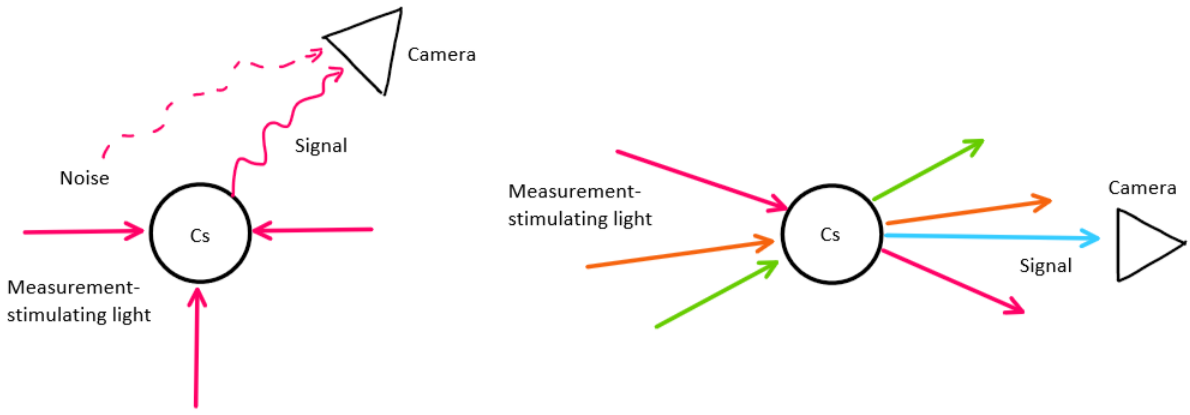

Figure 1.1: A graphical representation of the two measurement schemes we've introduced. On the left is measurement by resonance fluorescence, where the light used to stimulate the measurement has the same frequency as the signal, introducing a potential for noise. On the right is the proposed FWM-based measurement scheme, which stimulates measurements using three frequencies unique from the generated fourth frequency (blue), allowing us to filter out just the signal light for a less-noisy measurement.

One proposal to make qubit measurements less noisy is to measure them using a four-wave mixing (FWM) process, which would allow the measurement photon to have a frequency distinct from any other in the system. With a narrow bandpass filter centered around the measurement frequency, it would be possible to filter out all light in the system that doesn't include measurement results, and the only signals the camera or photodetector collects would be from measurement, eliminating ambiguity about the source of the collected light. A simple graphical representation of the difference between measurement by resonance fluorescence and a hypothtical FWM-based measurement scheme is shown in Figure 1.1.

This proposal has merit, but it is untested. So, this thesis set out to determine if a FWM scheme is a viable method for trapped-atom qubit measurement. The primary goal was to develop a model which would calculate the efficiency of the FWM process stimulated in a trapped atom qubit. In the future, this would help to conclude if the proposal is a viable alternative to measurement by resonance fluorescence by indicating if the resulting signal is sufficiently strong for given input laser powers.

To develop the model, we used a combination of analytical and numerical strategies, first finding an analytical solution to the wave equation for the field generated by the FWM process in terms of the system's density matrix element. Then, we used the QuTIP Python library to numerically determine the relevant density matrix element in the steady state. The result is a set of Python scripts which can plot relationships between the intensity of the

FWM signal and various system parameters, and return explicit values for the efficiency of the FWM process and the optical power of its generated signal in the trapped-atom system.

The thesis is organized as follows: In Chapter 2, we outline some theory used to develop the model; in Chapter 3, we discuss how we constructed the model; in Chapter 4, we present how we tested the model and explain why we feel confident in it; in Chapter 5, we apply the model to a hypothetical cesium system to demonstrate how it might be used to analyze the viability of FWM-based measurement in a specific system, and in Chapter 6, we outline some of the next steps required to make the model more robust.

Chapter 2

Theoretical Foundation

2.1 The Structure of a Cesium-Atom Qubit

One of the most important things to understand before attempting to model FWM dynamics in a trapped-atom qubit is how the qubit is structured. Many different atoms can be used as qubits, but for our purposes we'll be focusing on cesium, whose D2 line structure is commonly exploited for many applications, including for our qubit, shown in Figure 2.2.

A qubit must have a $|0\rangle$ and a $|1\rangle$ state. In our cesium system, we define these states in terms of the hyperfine splitting of the $6S_{1/2}$ level, with $|0\rangle$ corresponding to the lower hyperfine level $F = 3$ and $|1\rangle$ corresponding to the upper hyperfine level $F = 4$, as shown in Figure 2.1.

For this thesis, we'll focus on the qubit measurement process. A very popular approach to measurement in the cesium system is called *measurement by resonance fluorescence* or

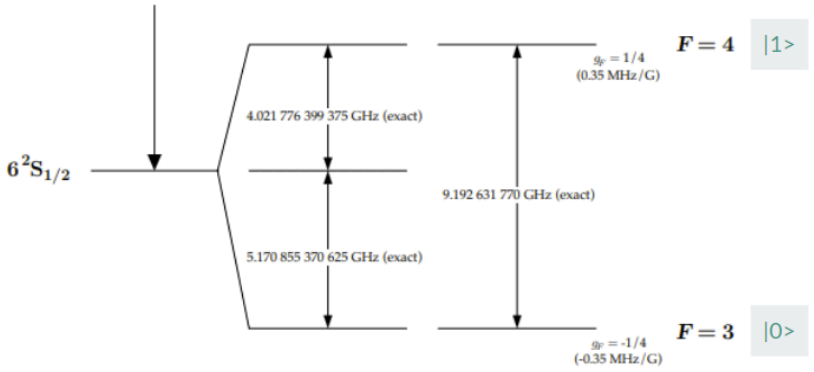

Figure 2.1: The states we use to define a cesium qubit, given by the hyperfine splitting of the ground state of the single valence electron in cesium. Adapted from [1].

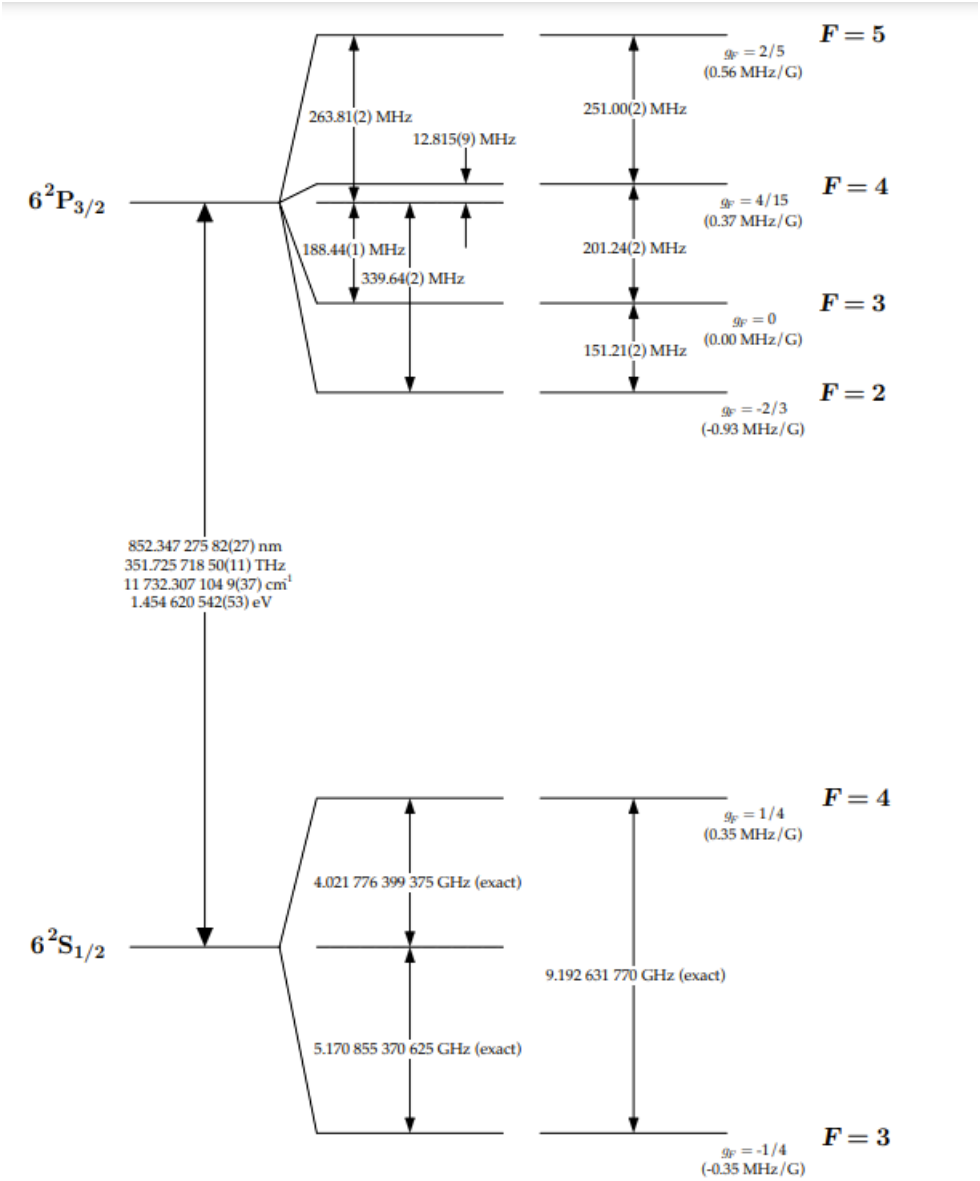

Figure 2.2: From [1], this is the D2 line of cesium, with ground state $6S_{1/2}$ and excited state $6P_{3/2}$.

resonance fluorescence readout, which we mentioned briefly in the introduction. Resonance-fluorescence readout is done by irradiating qubits with light that is on resonance with a transition between either the $|0\rangle$ or $|1\rangle$ qubit states and some excited state. Depending on the qubit's state, its single valence electron will either be excited and emit a photon by spontaneous emission, or it will remain in its initial state, where there is nowhere for it to decay to, and stay "dark". Then, by determining which qubits fluoresce and which don't, we can determine the state they were in. In the cesium system outlined above, the excited state used for resonance fluorescence measurement is most often the $6P_{3/2}$ state, and the cycling transition driven between this state and the $6S_{1/2}$ ground state is accomplished by 852 nm light. (The more-precise energies required are outlined in Figure 2.2.) So, when atoms fluoresce, they emit 852 nm signal photons.

One of the most pressing issues with measurement by resonance fluorescence is that the wavelength of the signal photons is already present elsewhere in the system. If you are using 852 nm photons to both excite your qubits and collect with a camera or photodetector to make conclusions about their state, you run the risk of measuring 852 photons which are *not* a product of spontaneous emission. In other words, there is a good chance that you are introducing significant noise into your measurements which is a product of 852 nm light having multiple uses in your system.

This is where the proposed FWM-based measurement scheme comes in: if we can use FWM to produce a signal photon which is not present anywhere else in the system, we can greatly reduce the amount of noise in our measurements with the introduction of an extremely narrow bandpass filter in front of the device used to collect the signal.

2.2 Four-Wave Mixing (FWM)

Four-wave mixing (FWM) is a third-order nonlinear optical process which generates a fourth frequency from three other frequencies in a nonlinear medium. FWM can be split into two categories: degenerate and non-degenerate FWM. Degenerate FWM requires three fields with two distinct frequencies while non-degenerate FWM requires three fields with unique frequencies. In this paper, we will focus on treating non-degenerate FWM.

We will not give a rigorous treatment of FWM but rather provide some intuition about the process and some conditions that must be met in experiment to stimulate it. Physically, non-degenerate FWM occurs when three photons of different frequencies are scattered and interact with the nonlinear medium to produce a fourth frequency. Essentially, the fourth frequency is a product of interference between the three incident frequencies.

Stimulating FWM is quite challenging as the laws of conservation of energy and momen-

tum lay out a strict set of requirements that must be met before it can occur. If the three incoming fields are named 1, 2, and 3, with 1 and 2 sharing the same sign on each quantity, and the generated field is named 4, the mathematical representation of these conditions is as follows:

$$\hbar\omega_4 = \hbar\omega_1 + \hbar\omega_2 - \hbar\omega_3 \tag{2.1}$$

$$\hbar\mathbf{k}_4 = \hbar\mathbf{k}_1 + \hbar\mathbf{k}_2 - \hbar\mathbf{k}_3 \tag{2.2}$$

$$\phi_4 = \phi_1 + \phi_2 - \phi_3 \tag{2.3}$$

where Equation 2.1 is the energy conservation equation, Equation 2.2 is the momentum conservation equation, and Equation 2.3 is the phase-matching condition.

Graphically, the conditions for energy and momentum conservation are shown in Figure 2.3. From both the mathematical and graphical representations of the conditions for FWM, it's clear that the two aspects of the FWM experiment that must be perfected to begin the process are the differences between the frequencies used and the angles at which the fields intersect.

However, just because conditions 2.1-2.3 are met does not mean that the resultant FWM process is as efficient as possible. To most efficiently stimulate FWM in an atomic system using lasers to produce the three incident fields, there is likely a very-specific set of detunings and laser powers required to maximize the optical power of the generated fourth frequency. This further complicates the task of achieving efficient FWM in an atom, as it introduces even more conditions that must be met if the goal is to make the process efficient. The model in described in the later chapters likely has the potential to streamline the process of determining which combination of system parameters will maximize the FWM efficiency, but as far as we're concerned, there is currently no straightforward way to do this.

2.3 Constructing the FWM System and Notation

In the very early stages of developing our model, we wanted to start with choosing an energy level structure that would permit us to stimulate FWM. Once we had the energy structure, we were able to know which frequencies were in our system, and thus allow us to fully realize its Hamiltonian. There are various energy level structures that allow for FWM such as the ladder/cascade-type structure, the double-lambda structure, and the diamond structure. We chose to use the diamond structure as it is particularly convenient in cesium, which we'll show briefly in the following paragraphs.

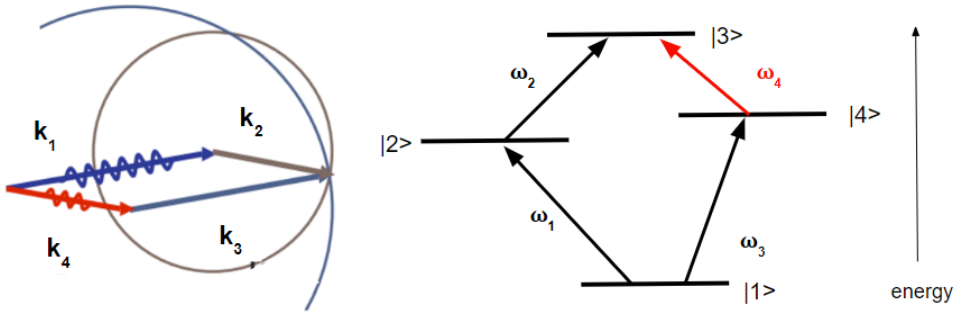

Figure 2.3: Graphical representations of conditions for FWM with wavevectors of applied fields $\mathbf{k}_1, \mathbf{k}_2, \mathbf{k}_3$ (black) and wavevector of generated field $\mathbf{k}_4$ (red). On the right is the energy conservation diagram, and the left is the momentum conservation diagram, adapted from [2]. In the momentum conservation diagram, the angle between $\mathbf{k}_1$ and $\mathbf{k}_4$ is set, and the two circles are mapped out by rotating $\mathbf{k}_2$ and $\mathbf{k}_3$ about the endpoints of the fixed vectors. The intersections of the two circles are solutions to the momentum conservation (and thus phase-matching condition.)

There are many different naming conventions used by authors of papers describing FWM in atomic systems with a diamond-type structure, but we've chosen to use a set of conventions adapted from [3] because the use of "pump" (p), "coupling" (c), "signal" (s), and "drive" (d) terminology makes the code that comprises the model a bit easier to read and work with. The energy level diagram demonstrating this naming convention is shown in Figure 2.4.

If you are familiar with cesium, you might notice that Figure 2.4 has a structure that could be easily replicated in cesium. Figure 2.5 makes this similarity a bit more obvious by arranging the energy levels in cesium in the diamond configuration. This is perhaps the most clear explanation for why a four-wave mixing scheme would lend itself measuring cesium qubits: FWM can be stimulated with an energy level structure that matches that of a cesium qubit nearly exactly. In cesium, you can choose $|1\rangle$ to be $6S_{1/2}$, $|2\rangle$ as $6P_{3/2}$, and $|4\rangle$ to be $6P_{1/2}$, the transitions between which have frequencies that are easily accessible using commercially-available semiconductor lasers, and are likely already present in a cesium qubit-based quantum information system. Then, all that's left is to choose is a $|3\rangle$ state, which is somewhat flexible, limited only by the energy level structure of cesium and possible laser locking mechanisms. Two such choices for $|3\rangle$ are the $6D_{3/2}$ level, used by [4] and shown in Figure 2.5, which would yield an 876 nm FWM signal, and the $8S_{1/2}$ level, used by [5], which would yield a 752 nm FWM signal when used in the diamond configuration.

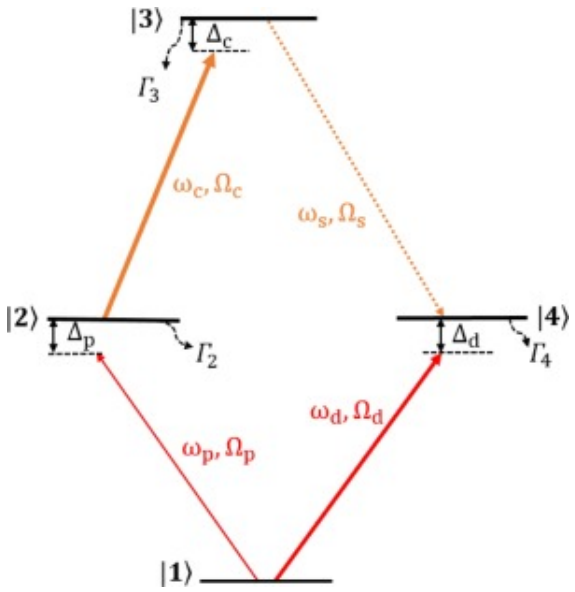

Figure 2.4: Energy level diagram featuring the naming conventions we'll use in this thesis, from [3]. Note that the p, c, s, d subscripts refer to the pump, coupling, signal, and drive transitions, respectively. ω_n refers to the transition frequency, Ω_n is the Rabi frequency, and Δ_n is the detuning, all of the n-th transition. Γ_m refers to the decay rate of the m-th state.

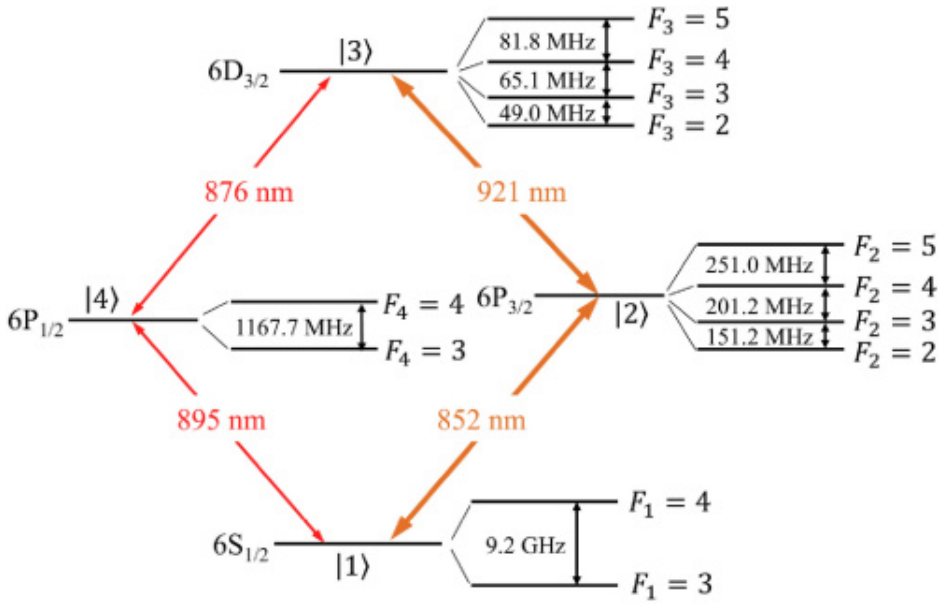

Figure 2.5: Example of a diamond energy level structure in cesium, where $|1\rangle$ is the ground state of cesium's valence electron, $|2\rangle$ is the $6P_{3/2}$ level we discussed above, $|4\rangle$ is the $6P_{1/2}$ level, which is the excited state in cesium's D1 line, and $|3\rangle$ is the $6D_{3/2}$ level. The $|1\rangle > |2\rangle$ and $|1\rangle > |4\rangle$ transitions are all accessible using very-common semiconductor lasers. From [4].

2.4 Density Matrix Formalism

In introductory quantum mechanics coursework, it's very common to work with quantum systems in *pure states*. When a quantum system is in a pure state, we know its state precisely. It might be a basis state or a linear combination of basis states, but whichever it is, we know its state well enough to prepare other systems in that exact same state. For example, a pure state of a spin-1/2 particle could be $|\psi\rangle = \frac{1}{\sqrt{2}}(|\uparrow\rangle + |\downarrow\rangle)$ in the standard basis. In this case, the state is well-known and if we wanted to, we could make lots of copies of this system. To be more mathematically rigorous, a pure state can be represented by *one* vector in the state space (the Hilbert space containing all the state vectors that the system could possibly be described by). This is why both basis states and linear combinations of basis states are pure states: by the definition of a basis, they are both contained within the state space.

Unfortunately, in most laboratory or 'real life' settings, it is not so easy to write out the state of the system. In this case, the state of the system is called a *mixed state*, and it is not a single vector in the state space but rather an ensemble of pure states, or a set of pure states the system *could* be in, along with their corresponding classical probabilities. This ensemble can be denoted as $\{(|\psi_i\rangle, p_i)\}$, where p_i is the probability that the system is in pure state $|\psi_i\rangle$. Griffiths and Schroeter describe the need to work with mixed states as a product of our own ignorance about the system, which itself is often a result of interactions with the environment [6]. (This type of system is called an *open quantum system.*) The premise of this thesis is to model a quantum system (an atom) whose state is affected by its environment (applied external electromagnetic fields), so establishing a mathematical foundation for working with mixed states is essential to the development of our model.

It's necessary to introduce 'new' mathematics when working with mixed states because the equations governing pure states and mixed states are not the same. Whereas the time evolution of pure states is described by the Schrödinger equation, the time evolution of mixed states of a closed system is governed by the Liouville-von Neumann equation (Equation 2.4).

$$\dot{\rho} = -i[H, \rho] \tag{2.4}$$

The H in Equation 2.4 is a standard Hamiltonian, but ρ is something not present in the Schrödinger equation: it's called the *density operator* and it's the foundation for the *density matrix formalism* of quantum mechanics. It can be considered a probability distribution of quantum states. The density operator is defined as follows:

$$\hat{\rho} = \sum_k p_k |\psi_k\rangle\langle\psi_k| \tag{2.5}$$

Once a basis is specified, the density operator is often called the *density matrix* whose elements are given by

$$\rho_{i,j} = \sum_k p_k \langle e_i|\psi_k\rangle\langle\psi_k|e_j\rangle \tag{2.6}$$

where e_i and e_j are basis vectors for the chosen basis [6]. Then, the density matrix can be constructed for some system in a mixed state. The diagonal elements in the density matrix are called *populations* and the off-diagonal elements are called *coherences* or *coherence elements*, which will be particularly useful to know for the later sections of this thesis [7]. Since the density matrix completely describes the system, we can use it and the Liouville-von Neumann equation to determine how a closed system in a mixed state evolves with time.

2.5 The Lindblad Master Equation

The Lindblad Master Equation is a tool physicists can use to understand the evolution of open quantum systems, which are quantum systems that are interacting with their environment. One of the most prominent examples of an open quantum system is that of an atom undergoing decay [7]. The interactions that cause this decay can vary: it might be due to an interaction between the atom and the surrounding vacuum state, or it might be due to an interaction between the atom and nearby electromagnetic fields.

This section will not focus on the derivation of the Lindblad master equation (this is done in multiple ways in [7]) but it will provide enough background to show more generally where it comes from and to introduce some of the relevant approximations made. All solving of the Lindblad master equation done for this thesis uses a Python library called QuTIP, which has a Lindblad master equation-solving function called `mesolve`, which is detailed more thoroughly in Chapter 3. `mesolve` makes some approximations that allow the Lindblad master equation to be written as follows:

$$\dot{\rho}(t) = -i[H(t), \rho(t)] + \frac{1}{2}\sum_n \left[2C_n\rho(t)C_n^\dagger - \rho(t)C_n^\dagger C_n - C_n^\dagger C_n\rho(t)\right] \tag{2.7}$$

where $H(t)$ is the system's Hamiltonian, which for this thesis is not time-dependent, and $\rho(t)$ is the system's density matrix. So, the Lindblad master equation gives the time evolution of the density matrix and thus the time evolution of the system's state.

You might notice that the first term in the Equation 2.7 is the right-hand side of the Liouville-von Neumann equation introduced in Section 2.4. This is because the Liouville-von Neumann equation describes the time-evolution of a closed quantum system in a mixed

state, but the Lindblad master equation has extra terms that factor in the effects of the environment, the existence of which make the quantum system *open*. These extra terms are included in the sum of Equation 2.7, and the new operator in the sum is called a *collapse operator*. The collapse operators describe how the system and its surroundings interact and have the form $C_n = \sqrt{\gamma_n} A_n$, where A_n "are the operators through which the environment couples to the system" and γ_n are their corresponding rates [8].

The QuTIP guide ([8]) notes that there are four primary approximations that must hold for a system if it's to be well-modeled by `mesolve`. The first is *separability*, or that the initial state has no correlation to its surroundings. The second is the *Born approximation* which requires that this separability remains throughout the entire period of evolution and that the state of the environment does not significantly change as a result of the interaction with the system. This second condition can be thought to be met if the environment is much larger than the system and the interaction is weak. The third approximation is the *Markov approximation*, which requires that the time scale of the environment's decay is much shorter than that of the system dynamics, and the fourth approximation is the *secular approximation*, which requires that the fast-rotating terms in the Hamiltonian can be neglected. Each of these approximations is appropriate to make in a trapped-atom system interacting with external fields, so we can use QuTIP to solve the Lindblad master equation for our system.

Chapter 3

Constructing the Model

Recall that the goal of this project is to create a model for FWM efficiency when FWM is stimulated in a trapped-atom system. There are two approaches to modeling FWM dynamics in a trapped atom that we considered throughout the development of this project, which we'll call the "proportionality approach" and the "explicit approach". The proportionality approach contains the basic relationships between FWM efficiency and system parameters, and the explicit approach is an extension of it in the sense that it allows us to turn these qualitative relationships into quantitative ones. Both approaches are relevant to understanding how we tested our model, so it is important to understand the details and development of each, which is what the first part of this chapter will focus on. The second half of the chapter will go into more detail about how we developed the model in accordance with these approaches and the tools we used to produce our results.

3.1 The Proportionality Approach

The development of our model began with this approach, inspired by [3] and [9], which we've called the Proportionality Approach because it's based on the fact that the FWM signal intensity, I_{FWM}, obeys the following proportionality relation:

$$I_{FWM} \propto |\rho_{43}|^2 \tag{3.1}$$

where ρ_{43} is the 43-th element of the density matrix that describes our system in the steady state. Conceptually, you can think of this element as telling us how 'coherent' the FWM process is along the $|3\rangle$ to $|4\rangle$ transition. If ρ_{43} is larger, the process is more coherent so it will yield a greater number of photons and thus a more intense signal. If ρ_{43} is smaller, the process is less coherent and cannot produce signal photons as effectively, meaning we get a

weaker signal.

Because Expression 3.1 tells us about what the signal intensity is proportional to rather than its magnitude, it only makes sense to use it in a context where we are comparing signal intensities from systems with different parameters. Although this is not clearly aligned with our goal of calculating FWM efficiency, it is a useful relationship to model to provide an educated guess about which parameters might maximize the intensity of the generated signal, and as we'll see later, it was a convenient starting point for testing our model.

For now, we will choose to take this proportionality relationship as a true without proving it; we'll show that it's true later in Section 3.4. This organizational choice might seem counterintuitive but I'd argue that describing the approaches in this order makes sense because this is the point from which we started the development of the model, and it was also the first result we tested the model against, which is detailed in Section 4.1.

3.2 The Explicit Approach

Unlike the proportionality approach, what we've called the 'explicit approach' allowed us to calculate an explicit expression for the FWM efficiency rather than some relationship in arbitrary units. This approach is considerably more mathematically involved and is something we quasi-derived rather than finding in a few papers. For now, we'll present the expression we derived and the derivation will be presented in Section 3.4. As such, the expression for the FWM signal intensity we found via the Explicit Approach is as follows:

$$I_{FWM} = 2\pi^2 cn\epsilon_0 \cdot P_s^2 \tag{3.2}$$

where P_s is the atomic polarization density resulting from the generation of the signal light, n is the refractive index of the surroundings (set to 1) and k is the wavenumber. The derivation of this will be given in Section 3.4.

Of course, Equation 3.2 is not an efficiency. To get an expression for the FWM efficiency as desired, we defined it as

$$\epsilon_{FWM} = \frac{I_{FWM}}{I_d} \tag{3.3}$$

where I_{FWM} is the FWM signal intensity and I_d is the intensity of the drive beam, which is most commonly used in the definition of FWM efficiency in published literature, although one could define the efficiency using the intensity of the pump or coupling beams if that is more convenient.

Then, Equation 3.2 substituted into Equation 3.3 yields the efficiency expression we set

out to find at the beginning of the project. This model was tested against experimental data, and the results can be found in Section 4.2.

3.3 Constructing the Proportionality Model

Up to this point, I've presented the approaches we used to model the FWM dynamics without explanation or proof. In the next two sections, I'll talk about the theoretical process used to get our results before commenting on the tools used to perform the model's calculations.

In this section, I'll describe how we constructed our initial model, which was based on the proportionality approach. Recalling Equation 3.1, it's clear that to model the proportionality relationship, it suffices to solve for ρ_{43}, the 4,3-th element of the system's density matrix when the system is in the steady state.

The first step in developing this model was to notice that the quantum system consisting of the trapped atom is an open system: it is very much interacting with its environment, which we can consider to be the incident laser beams and the surrounding vacuum. Given this, we decided to approach solving for ρ_{43} by solving the Lindblad master equation for the system, setting $\dot{\rho} = 0$ to get the steady state solution, and solving for the coherence element we're interested in from there.

However, as we hinted in Section 2.4, finding analytical solutions to the dynamics of mixed-state systems (and thus open systems) is extremely challenging even for two-level systems, let alone four-level systems. So, we sought to find a method that would offer a numerical solution to the Lindblad master equation and settled on using a Python library called QuTIP to perform this calculation.

3.3.1 QuTIP's `mesolve` Function

The QuTIP function that was essential to the development of both of our models is called `mesolve`. Normally, it's unnecessary to describe code in so much detail, but it's useful to understand the parameters that `mesolve` requires to incorporate the correct physics into the model.

`mesolve` offers a numerical solution to the Lindblad master equation. For our model, we needed to provide the function with four parameters:

1. the system's "total" Hamiltonian, H_{tot}
2. the initial state of the system $|\psi_0\rangle$, provided as a density matrix
3. a list of times (after $t = 0$) at which we want to know the state of the system

4. a list of collapse operators

After calling `mesolve` with this set of input parameters, the program evolves the initial state in agreement with the Lindblad master equation and the given parameters until each time in the provided list. Once the system has evolved for some time included in parameter (3), the program saves the state of the system at that time (its density matrix) to an array and returns the array after the system has evolved for the longest time included in parameter (3). So, the output of `mesolve` is an array of density matrices that describe the state of the system at the times we are interested in.

Then, all that is left to do to find ρ_{43} is to 'take out' that element from one of the density matrices returned once the system is in the steady state. Next, I'll briefly outline how we constructed the parameters to ensure that `mesolve` was modeling the physics we were interested in.

Constructing the Hamiltonian

The QuTIP guide explains that the Hamiltonian passed to `mesolve` should be a "total" Hamiltonian, defined by

$$H_{tot} = H_{sys} + H_{env} + H_{int} \tag{3.4}$$

where H_{sys} is the Hamiltonian we would use if our atom was completely isolated (i.e. a closed system), H_{env} is the Hamiltonian of the surrounding environment, and H_{int} is the Hamiltonian representing the interactions between the atom and the environment [8]. So, to construct the relevant Hamiltonian, it's easiest to do it in parts, with each part corresponding to a term in the sum.

Before constructing the total Hamiltonian in three parts, we first need to choose a basis for our system, which is as follows:

$$|1\rangle = \begin{pmatrix} 1 \\ 0 \\ 0 \\ 0 \end{pmatrix}, \; |2\rangle = \begin{pmatrix} 0 \\ 1 \\ 0 \\ 0 \end{pmatrix}, \; |3\rangle = \begin{pmatrix} 0 \\ 0 \\ 1 \\ 0 \end{pmatrix}, \; |4\rangle = \begin{pmatrix} 0 \\ 0 \\ 0 \\ 1 \end{pmatrix} \tag{3.5}$$

Now that the basis of the system has been established, we can continue to solve for H_{tot}. As we derive expressions for the various Hamiltonians, we will be treating our system as a semiclassical one: that is, that our atom, which is a quantum system, is interacting with a classical field. Note that none of the Hamiltonians in the following sections will include a factor of $\hbar$, as these are omitted in parameters passed to QuTIP functions.

First, solve for H_{sys}, which have the energy of each level along the diagonal and zeroes everywhere else. (Refer to Figure 2.4 to recall the naming conventions used.) Then, calling the frequency of the ground state ω_1, and omitting the factor of $\hbar$ that would be included in 'normal' contexts, we have

$$H_{sys} = \begin{pmatrix} \omega_1 & 0 & 0 & 0 \\ 0 & \omega_1 + \omega_p - \Delta_p & 0 & 0 \\ 0 & 0 & \omega_1 + \omega_p - \omega_{21} + \omega_c - \omega_{23} & 0 \\ 0 & 0 & 0 & \omega_1 + \omega_d - \omega_{14} \end{pmatrix} \tag{3.6}$$

We can choose to set ω_1 to zero since it is a common offset shared by each level, and we can simplify Equation 3.6 by substituting the definitions of the various detunings as follows:

$$H_{sys} = \begin{pmatrix} 0 & 0 & 0 & 0 \\ 0 & \Delta_p & 0 & 0 \\ 0 & 0 & \Delta_p + \Delta_c & 0 \\ 0 & 0 & 0 & \Delta_d \end{pmatrix} \tag{3.7}$$

Take Equation 3.7 to be the H_{sys} we use in the H_{tot} expression.

Next, solve for H_{int}, which is considerably more involved. It's likely easiest to think about the construction of this operator from a more conceptual perspective. We know that H_{int} describes the interaction between the environment (the incident laser beams) and the system (the atom). For the purposes of Hamiltonian construction, we can think of the interaction as a mechanism that drives Rabi oscillations between pairs of adjacent states. Essentially, this is 'taking care' of two process occurring simultaneously in the system: excitations and decay by stimulated emission. Then, H_{int} only needs to describe the Rabi oscillations, which is well-documented for two- and three-level systems in [10].

We can use the procedure for constructing Hamiltonians describing Rabi oscillations in two- and three-level systems for constructing that of our four-level system. If we only had a two-level system with $|1\rangle$ and $|2\rangle$, ignoring the phase of the laser beam and using the rotating wave approximation (RWA), we have from [10] that

$$(H_{sys})_2 = \begin{pmatrix} 0 & \Omega_p/2 \\ \Omega_p^*/2 & \Delta_p \end{pmatrix} \tag{3.8}$$

This is indicative of a pattern that holds for systems of greater size: essentially, for a Rabi oscillation stimulated from state m to state n with $m < n$, the m, n-th element of H_{int} is given by $\Omega_{mn}/2$ and the n, m-th element is $\Omega_{mn}^*/2$. To construct H_{int} in its entirety, consider where the Rabi oscillations can be stimulated:

- from $|1\rangle$ to $|2\rangle$ and vice versa
- from $|2\rangle$ to $|3\rangle$ and vice versa
- from $|1\rangle$ to $|4\rangle$ and vice versa

So, there will be six nonzero elements in H_{int}. Notice that there are no Rabi oscillations between states $|3\rangle$ and $|4\rangle$ because there is no incident laser whose frequency is on resonance with the $|3\rangle > |4\rangle$ transition. Then, for example, the $1,4$-th element of H_{int} must be $\Omega_d/2$ and the $4,1$-th element must be $\Omega_d^*/2$. Putting together what we know, we have

$$H_{int} = \begin{pmatrix} 0 & \Omega_p/2 & 0 & \Omega_d/2 \\ \Omega_p^*/2 & 0 & \Omega_c/2 & 0 \\ 0 & \Omega_c^*/2 & 0 & 0 \\ \Omega_d^*/2 & 0 & 0 & 0 \end{pmatrix} \tag{3.9}$$

Then, the last step in forming H_{tot} is to find H_{env}. If you list the processes happening in the atomic system while we attempt to stimulate FWM, you'll find that the atom's valence electron is either being excited, emitting a photon by stimulated emission, or emitting a photon by spontaneous emission. The first two processes are described by H_{int}, but spontaneous emission remains to be included in the modeling. To do this, we use collapse operators, which are described by QuTIP to be the product $\sqrt{\gamma_n}A_n$, where A_n is the operator through which the system couples to the environment and γ_n is the rate at which the operator 'works' [8]. In our system, the collapse operators are responsible for unwanted decay, which is that done via spontaneous emission.

This is just to say that the only dynamics that remain to be modeled are taken care of by the collapse operators, which are constructed later. So, the H_{env} is zero because there's nothing 'going on' in the environment that needs to be included in H_{tot}, because all of the relevant details pertaining to the environment are included in the collapse operators.

So, H_{tot} for the trapped-atom system is simply the sum of H_{int} and H_{sys}:

$$\boxed{H_{tot} = \begin{pmatrix} 0 & \Omega_p/2 & 0 & \Omega_d/2 \\ \Omega_p^*/2 & \Delta_p & \Omega_c/2 & 0 \\ 0 & \Omega_c^*/2 & \Delta_p + \Delta_c & 0 \\ \Omega_d^*/2 & 0 & 0 & \Delta_d \end{pmatrix}} \tag{3.10}$$

which is consistent with that presented by Nguyen and Tsai.

The Initial State of the System

Since we want to model the efficiency of a FWM process that begins with an atom in the $|1\rangle$ state, it's the obvious choice for the initial state parameter. Since QuTIP requires the initial state to be a density matrix, the actual parameter passed is

$$\boxed{|\psi_0\rangle = \begin{pmatrix} 1 & 0 & 0 & 0 \\ 0 & 0 & 0 & 0 \\ 0 & 0 & 0 & 0 \\ 0 & 0 & 0 & 0 \end{pmatrix}} \tag{3.11}$$

Evaluation Times

The main thing that we need to determine when constructing a list of evaluation times to send to `mesolve` is when the steady state begins. There are more mathematically rigorous ways to do this, but for the sake of time, we did this by running `mesolve` with parameter (3) being a long interval containing approximately 100 evenly-spaced times. Then, we used the results to plot ρ_{43} as a function of time and noted when the curve flattened out, indicating that the system was in the steady state. Then, when we ran `mesolve` with the intention of using the results for the model, we made parameter (3) a 50-item list of evaluation times, the final of which was a time safely in the steady state. For example, if we found that the steady state began after six seconds of evolution in my test run, we would ask `mesolve` to evolve the system for ten seconds. Then we would take ρ_{43} from the 50th density matrix that the function returned to ensure that the coherence element reflected the system when it was in the steady state.

Constructing the Collapse Operators

To construct the collapse operators, note the possible spontaneous emission pathways:

- $|2\rangle$ to $|1\rangle$
- $|3\rangle$ to $|2\rangle$ OR $|4\rangle$
- $|4\rangle$ to $|1\rangle$

Then, we should have four collapse operators:

$$C_{21} = \begin{pmatrix} 0 & \sqrt{\Gamma_2} & 0 & 0 \\ 0 & 0 & 0 & 0 \\ 0 & 0 & 0 & 0 \\ 0 & 0 & 0 & 0 \end{pmatrix}, C_{32} = \begin{pmatrix} 0 & 0 & 0 & 0 \\ 0 & 0 & \sqrt{\Gamma_3} & 0 \\ 0 & 0 & 0 & 0 \\ 0 & 0 & 0 & 0 \end{pmatrix},$$

$$C_{34} = \begin{pmatrix} 0 & 0 & 0 & 0 \\ 0 & 0 & 0 & 0 \\ 0 & 0 & 0 & 0 \\ 0 & 0 & \sqrt{\Gamma_3} & 0 \end{pmatrix}, C_{41} = \begin{pmatrix} 0 & 0 & 0 & \sqrt{\Gamma_4} \\ 0 & 0 & 0 & 0 \\ 0 & 0 & 0 & 0 \\ 0 & 0 & 0 & 0 \end{pmatrix}$$

Notice that for each collapse operator C_{nm} representing the decay by spontaneous emission from the n-th level to the m-th, the only nonzero element is the mn-th. This means that if you apply C_{nm} to $|n\rangle$, the result will be $|m\rangle$, which is consistent with what we would expect for a spontaneous emission process. Since this mechanism is only concerned with the populations (diagonal elements) of the density matrix, it suffices to use ket notation for the basis elements to explain the action of the collapse operators.

As it is quite challenging to find data for decay rates along specific pathways in cesium, we chose to define γ_n as $\Gamma_n = 1/\tau_n$, where τ_n is the lifetime of the state in seconds. In addition, it's important to note that the Lindblad master equation is not linear in collapse operators, which means that each operator must be considered and sent to `mesolve` separately rather than in a sum similar to that of H_{tot}.

Now that we've outlined how to define each `mesolve` parameter, modeling Expression 3.1 is extremely straightforward. To get ρ_{43}, one needs to run `mesolve` with the above parameters, then extract the $4,3$-th element from the very last density matrix produced by the function to ensure that it's taken from a steady-state solution. From there, it is easy to square ρ_{43}, and to investigate various relationships between the system parameters such as detunings and Rabi frequencies (effectively, laser intensities) and the relative FWM signal intensities.

This was the first model we constructed, but it was not the last– rather, we built on this framework to construct the explicit model, which is detailed in the following section.

3.4 Constructing the Explicit Model

As previously mentioned, the proportionality approach was insufficient for meeting our goal of deriving an explicit expression for the FWM efficiency. So, in this section I'll outline my derivation of this explicit expression for FWM efficiency in a trapped atom, up to the density matrix element, which is still solved for numerically using QuTIP.

The first step in the derivation is to derive an expression for the electric field of the generated FWM signal, which can then by converted to an intensity to be used in an efficiency expression. My derivation for the electric field is very similar to that done in [11], with some adjustments made since the trapped atom system does not have a thermal distribution or a meaningful length scale like a vapor cell.

Willis, et al. give the wave equation for an electromagnetic field propagating in an atomic medium in the z-direction under the slowly-varying amplitude approximation as

$$\partial_z E_i = 2\pi|k|ie^{-ik_i z}P_i(z) \tag{3.12}$$

where $P_i(z)$ is the polarization density in the atom generated by the i-th frequency and $|k_s|$ is the magnitude of the electric field's wavenumber k_s, defined as $2\pi/\lambda_s$ [11]. Given that each light source in the system that we might want to model with Equation 3.12 is either a laser or an atom, the slowly-varying amplitude approximation is appropriate as each of these sources have small linewidths (narrow spectra).

We want to solve for E_s, the electric field of the generated signal, so the specific equation we want to solve is

$$\partial_z E_s = 2\pi|k_s|ie^{-ik_s z}P_s(z). \tag{3.13}$$

Before integrating to solve for E_s, we should find an expression for $P_s(z)$, the polarization density in the atom coming from its interaction with the signal photons. [Willis] notes that the polarization and the density matrix are related by $P = N\,\mathrm{Tr}(\rho\mu)$ where N is the atomic number density and μ is the atom's dipole moment. As we're only interested in $P_s(z)$, this becomes

$$P_s(z) = N\mu_{34}\rho_{43} \tag{3.14}$$

Defining N to be the reciprocal of the atomic volume and r to be the orbital radius of the valence electron, we have

$$\boxed{P_s = \frac{3}{4\pi r^3} \cdot \mu_{34}\rho_{43}} \tag{3.15}$$

Notice that P_s actually has no z dependence unlike in [11] where it *does* have z-dependence to account for the attenuation that occurs as the beams travel through a vapor and are absorbed by many atoms rather than just one in the trapped-atom case. The z-dependence in the exponential is also easy to ignore once you use the electric field to calculate the corresponding intensity, so we will not describe that in any more detail for the trapped-atom system. Then the differential equation we want to solve becomes

$$\begin{aligned} \partial_z E_s &= 2\pi|k_s|ie^{-ik_s z}P_s \\ &= \frac{3}{2r^3} \cdot \mu_{34}\rho_{43} \cdot |k_s|ie^{-ik_s z} \end{aligned} \tag{3.16}$$

Before integrating, notice that the derivative of $e^{-ik_s z}$ is included in the wave equation. Since the exponential is the only term with z-dependence, the integral is quite nice to evaluate, yielding

$$\boxed{E_s = -\frac{3}{2r^3} \cdot \mu_{34}\rho_{43} \cdot e^{-ik_s z}} \tag{3.17}$$

Or, in terms of the atomic polarization density:

$$\boxed{E_s = -2\pi e^{-ik_s z} \cdot P_s} \tag{3.18}$$

Of course, this result only really holds because we care more about the magnitude of the electric field than we do about maintaining an expression for the field that reflects its 'true' structure as a wave. If this wasn't the case, we would have had to be more careful with equating k_s and $|k_s|$. As a result, we have an expression for the electric field of the generated FWM signal.

Now, we can use the expression for the resultant electric field to find an expression for the FWM intensity that we dealt with in the proportionality approach. Recall that

$$I = \frac{cn\epsilon_0}{2} \cdot |E|^2 \tag{3.19}$$

where n is the index of refraction of the material [12]. Then,

$$\begin{aligned} I_{FWM} &= \frac{cn\epsilon_0}{2} \cdot |-2\pi e^{-ik_s z} \cdot P_s|^2 \\ &= \frac{cn\epsilon_0}{2} \cdot 4\pi^2 \cdot P_s^2 \\ \boxed{I_{FWM} &= 2\pi^2 cn\epsilon_0 \cdot P_s^2} \end{aligned} \tag{3.20}$$

If you substitute the expression for P_s into Equation 3.20, it is obvious that the proportionality approach is a product of this derivation, rather than a completely distinct result:

$$I_{FWM} = 2\pi^2 cn\epsilon_0 \cdot \left(\frac{9}{16\pi^2 r^6} \cdot \mu_{34}^2 \cdot |\rho_{43}|^2 \right) \tag{3.21}$$

$$\boxed{I_{FWM} = \left(\frac{9cn\epsilon_0}{8r^6} \cdot \mu_{34}^2 \right) |\rho_{43}|^2} \tag{3.22}$$

Then, by Equation 3.22, the proportionality constant α for which $I_{FWM} = \alpha \cdot |\rho_{43}|^2$ is

$$\boxed{\alpha = \frac{9cn\epsilon_0}{8r^6} \cdot \mu_{34}^2} \tag{3.23}$$

Now, using Equations 3.3 and 3.22, we have an expression for the FWM intensity for the trapped-atom system:

$$\boxed{\epsilon_{FWM} = \frac{2\pi^2 cn\epsilon_0 \cdot P_s^2}{I_d}} \tag{3.24}$$

Finding Equation 3.24 was the goal of the thesis, but it will also be helpful to use these results to calculate an expression for the optical power of the FWM signal.

We have an expression for the FWM signal intensity, and we know that intensity is power per unit area A such that

$$P_{FWM} = I_{FWM} \cdot A \tag{3.25}$$

It remains to determine A, which we'll take to be the cross-sectional area of the generated beam. Since there's not a very nice way to predict what this might be, assume that the generated beam has a waist similar to the waists of the incident beams. In this thesis, we'll primarily assume that each beam has the same waist of 1 mm; in other situations a more complex approach to this problem might be required.

Then, $A = \pi w_0^2$ where w_0 is the beam waist, and

$$P_{FWM} = I_{FWM} \cdot \pi w_0^2 \tag{3.26}$$

$$= \left(\frac{9cn\epsilon_0}{8r^6} \cdot \mu_{34}^2 \right) |\rho_{43}|^2 \cdot \pi w_0^2 \tag{3.27}$$

$$\boxed{P_{FWM} = \left(\frac{9cn\pi\epsilon_0}{8r^6} \cdot \mu_{34}^2 \cdot w_0^2 \right) |\rho_{43}|^2} \tag{3.28}$$

Now, we have an expression for the intensity and the optical power of the generated FWM signal.

Chapter 4

Verifying the Model

After developing the model, we wanted to verify that it produced results we would expect. This proved quite challenging as we don't have experimental results of our own to use for verification, and I don't have the intuition necessary to predict the exact dynamics I would expect to see given a set of input parameters. So, we verified the model by comparing it to results from Nguyen and Tsai ([3]) and Willis et al. ([11]), which we'll call verification by qualitative methods and verification by quantitative methods, respectively.

4.1 Verification with Qualitative Methods

The most logical place to begin to verify the model seemed to be with the results from Nguyen and Tsai, who sought to model FWM dynamics for single, stationary atoms using what I've called the proportionality approach. I chose to start here because Nguyen and Tsai's paper included a wide selection of plots to recreate and their system was very similar to the one we want to model. It was also convenient to test the qualitative model first as it was less-rigourous and would more easily give us an idea of whether our approach was worth continuing to use.

There were three sets of plots from [3] that we wanted to replicate to verify our model: (1) FWM intensity as a function of pump or coupling detuning, (2) FWM intensity as a function of coupling and driving Rabi frequencies and pump detuning, and (3) FWM intensity as a function of pump detuning and equal coupling and driving Rabi frequencies, which we will call Sets 1, 2, and 3 moving forward.

4.1.1 Verification of Set 1

Set 1 consists of two plots, the first of which is a plot of FWM signal intensity as a function of the detuning of the coupling beam (Δ_c), and the second of which is a plot of the signal intensity as a function of the pump beam's detuning (Δ_p). Recall that in this model, the FWM intensity is proportional to the square of the $4,3$-th coherence element, ρ_{43}, in the steady state.

I figure that it will be easiest to show that our model's results are consistent with Nguyen and Tsai's by first presenting the published plots, then showing our own. So, Figure 4.1 shows Nguyen and Tsai's plots from Set 1, using the system parameters outlined in Table 4.1. Notice that when the coupling frequency is scanned, two peaks form at $\pm 14 \cdot 2\pi$ MHz, and when the pump frequency is scanned, four peaks form at approximately $\pm 14 \cdot 2\pi$ MHz and $\pm 26 \cdot 2\pi$ MHz, with dips at $\pm 20 \cdot 2\pi$ MHz.

Parameter	Value of Parameter for (a), in 2π MHz	Value of Parameter for (b), in 2π MHz
Δ_p	0	varied
Δ_c	varied	0
Δ_d	0	0
Ω_p	20	0.01
Ω_c	0.01	15
Ω_d	20	40
Γ_2	6.1	6.1
Γ_3	0.66	0.66
Γ_4	5.7	5.7

Table 4.1: System parameters used by [3] to plot Figure 4.1, which we used to verify our model.

Figures 4.2 and 4.3 show the plots our model produced using the same parameters as [3] shown in Table 4.1.

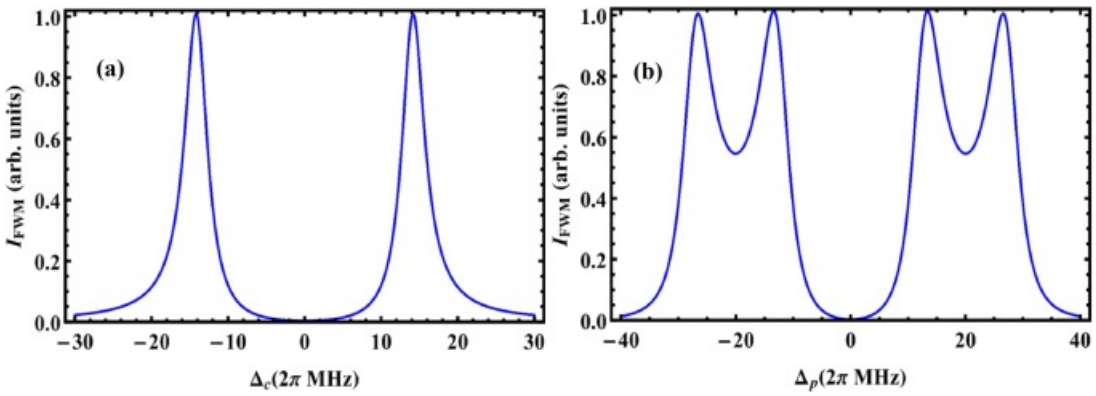

Figure 4.1: As Figures 2(a) and 2(b) from [3], these are the published plots of FWM signal intensity as a function of (a) coupling frequency detuning and (b) pump frequency detuning that we used to compare our model to. To see the relevant system parameters, see Table 4.1.

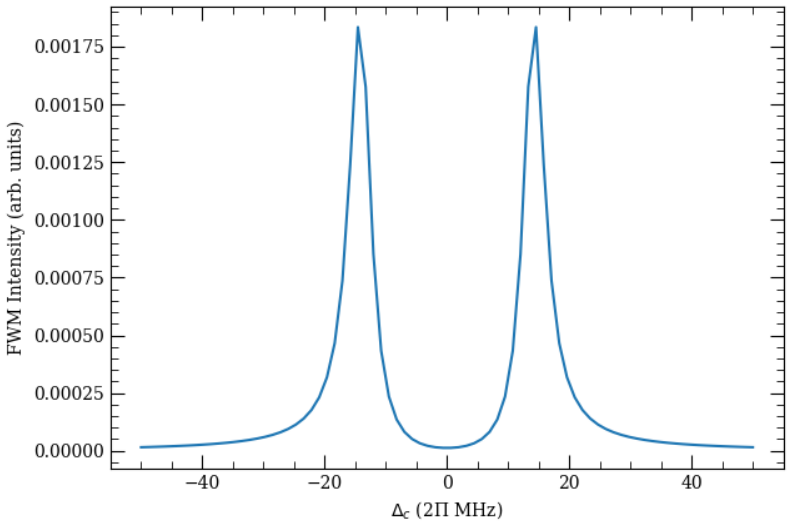

Figure 4.2: FWM signal intensity as a function of coupling beam detuning Δ_c produced by our model when given the system parameters shown in Table 4.1.

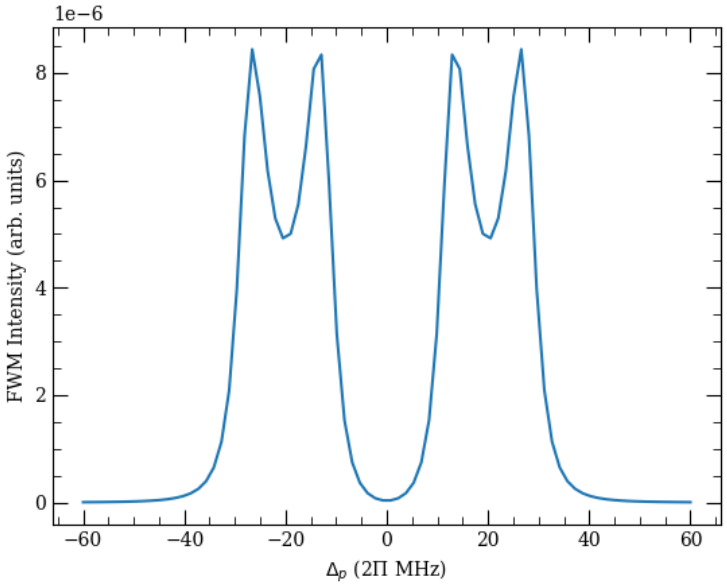

Figure 4.3: FWM signal intensity as a function of pump beam detuning Δ_p produced by our model when given the system parameters shown in Table 4.1.

It is clear that the plots from both Nguyen and Tsai (Figure 4.1) and our model (Figures 4.2, 4.3) have the same general shapes, but upon further inspection, it is also evident that the prominent peaks and dips occur at the same values of Δ_c and Δ_p. In addition, the relative amplitudes of the features are consistent between the results from our model and those from Nguyen and Tsai. This was the first published result we replicated with our model, which gave us hope that the model was demonstrating the dynamics we'd expect.

4.1.2 Verification of Set 2

Set 2 consists of four plots, each of which plot the FWM signal intensity against Δ_p/Γ_2, the ratio between the pump beam detuning and the decay rate of $|2\rangle$. For each plot, the Rabi frequency of the coupling beam Ω_c is fixed at a given value that differs between plots, and the Rabi frequency of the driving beam Ω_d is set to various half-integer multiples of Γ_2, producing the results shown in Figure 4.4, which use the system parameters outlined in Table 4.2.

For comparison, the results our model produced using the same system parameters (Table 4.2) are shown in Figures 4.5, 4.6, 4.7, and 4.8, which correspond to (a), (b), (c), and (d) in Figure 4.4, respectively.

Oncemore, there is good agreement between the published results (Figure 4.4) and the

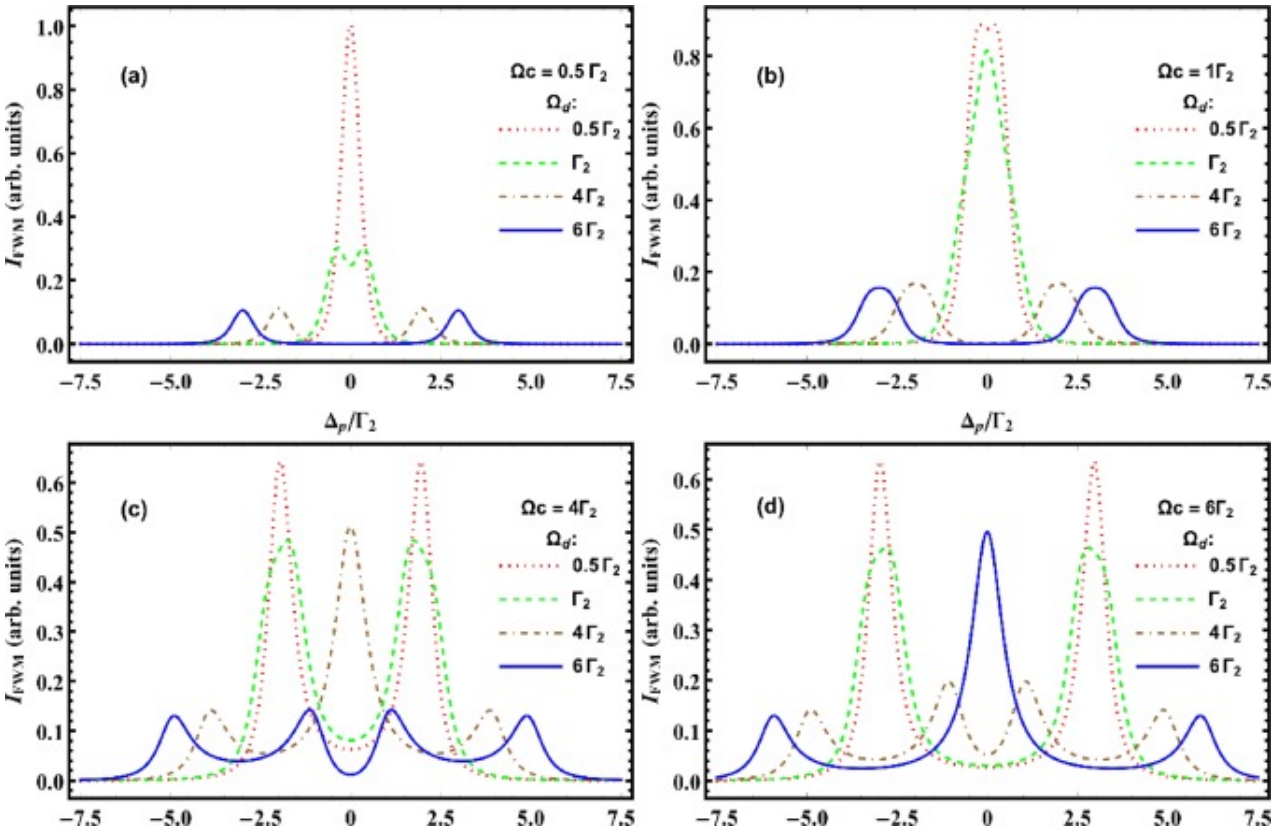

Figure 4.4: As Figures 4(a) through 4(d) from [3], these are the published plots of FWM signal intensity as a function of Δ_p/Γ_2. For each plot (a)-(d), Ω_c is fixed and noted in the upper right of the frame, and each curve corresponds to that generated by the system with a given Ω_d, given in the legend on the right of the frame. To see the relevant system parameters, see Table 4.2.

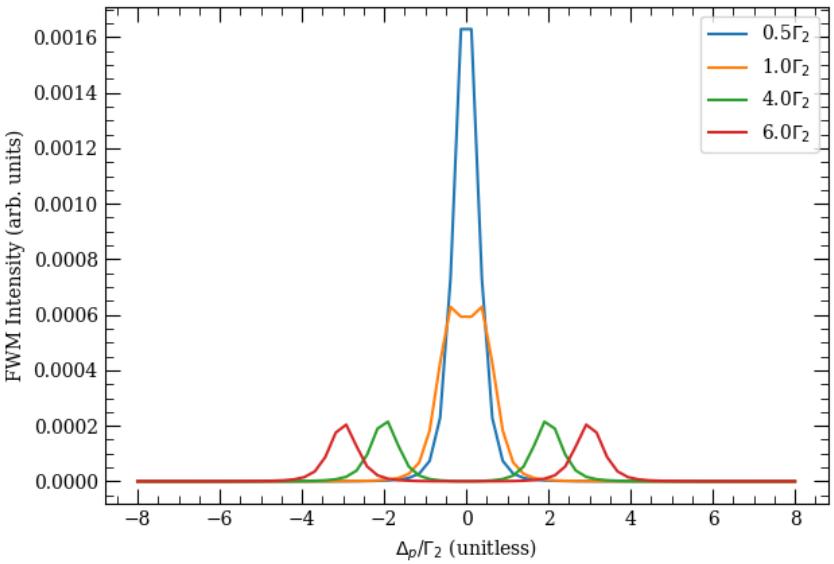

Figure 4.5: Plot of FWM signal intensity against Δ_p/Γ_2 with $\Omega_c = 0.5\Gamma_2$ and Ω_d shown in the legend on the right, produced by our model. This corresponds to (a) in Figure 4.4. To see all relevant system parameters, see Table 4.2.

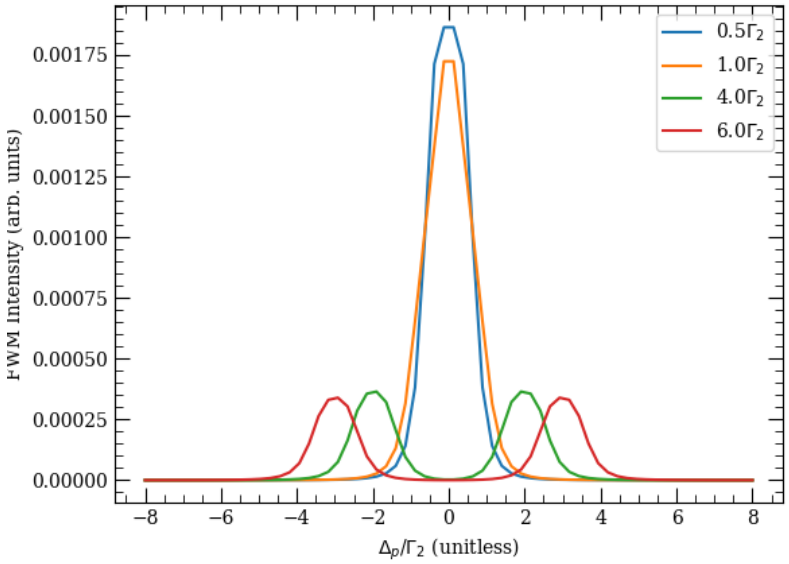

Figure 4.6: Plot of FWM signal intensity against Δ_p/Γ_2 with $\Omega_c = \Gamma_2$ and Ω_d shown in the legend on the right, produced by our model. This corresponds to (b) in Figure 4.4. To see all relevant system parameters, see Table 4.2.

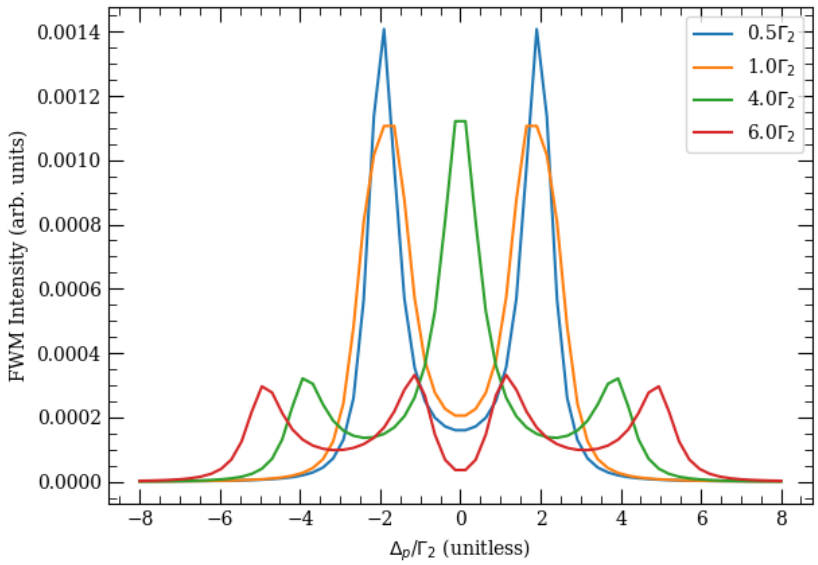

Figure 4.7: Plot of FWM signal intensity against Δ_p/Γ_2 with $\Omega_c = 4\Gamma_2$ and Ω_d shown in the legend on the right, produced by our model. This corresponds to (c) in Figure 4.4. To see all relevant system parameters, see Table 4.2.

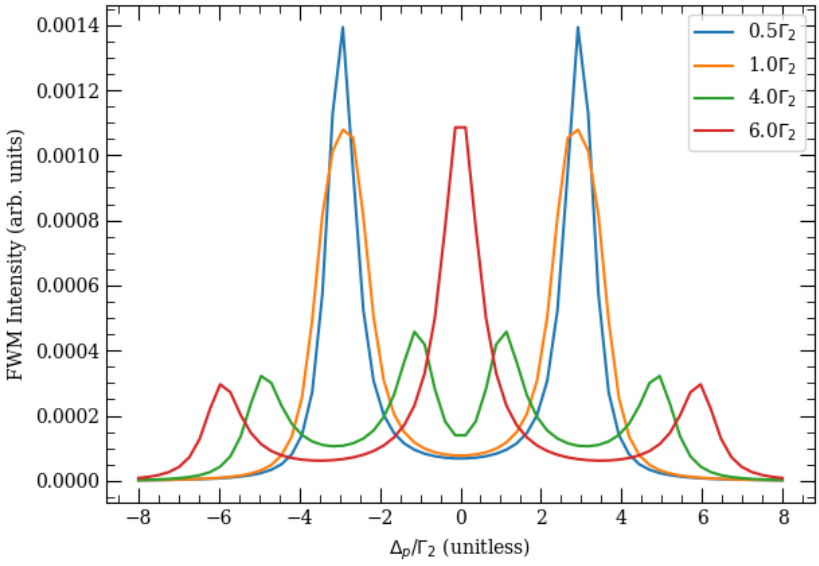

Figure 4.8: Plot of FWM signal intensity against Δ_p/Γ_2 with $\Omega_c = 6\Gamma_2$ and Ω_d shown in the legend on the right, produced by our model. This corresponds to (d) in Figure 4.4. To see all relevant system parameters, see Table 4.2.

Parameter	Value of Parameter for (a), in 2π MHz	Value of Parameter for (b), in 2π MHz	Value of Parameter for (c), in 2π MHz	Value of Parameter for (d), in 2π MHz
Δ_p	varied	varied	varied	varied
Δ_c	0	0	0	0
Δ_d	0	0	0	0
Ω_p	$0.01\Gamma_2$	$0.01\Gamma_2$	$0.01\Gamma_2$	$0.01\Gamma_2$
Ω_c	$0.5\Gamma_2$	Γ_2	$4\Gamma_2$	$6\Gamma_2$
Ω_d	see legends	see legends	see legends	see legends
Γ_2	6.1	6.1	6.1	6.1
Γ_3	0.61	0.61	0.61	0.61
Γ_4	6.1	6.1	6.1	6.1

Table 4.2: System parameters used by [3] to plot Figure 4.4, which we used to verify our model.

results produced by our model (Figures 4.5-4.8) for the same system parameters. Most notably, the relative amplitudes of the peaks in each plot are consistent between the published plots and those produced by our model. Additionally, the peaks appear at the same values of Δ_p/Γ_2 in the published plots and our model's plots.

This test was particularly important for understanding our model because of how the features look at $\Delta_p/\Gamma_2 = 0$: it's easy to notice that the nice, sharp peaks seen at this location in Figure 4.4 are not present in any of the plots generated by the model. There's a simple explanation for this. Since $\Delta_c = \Delta_d = 0$, the addition of the $\Delta_p = 0$ condition that's implied by $\Delta_p/\Gamma_2 = 0$ sets each detuning in the system to 0. When this is the case, the `mesolve` function in QuTIP that serves as the foundation of our model struggles to perform the required numerical integration. When the detunings are all zero, the compiler will time out even when we maximize the "options", which is how we can communicate to `mesolve` how to most efficiently perform its numerical integration.

Although the model struggles when all detunings are zero, we decided not to be too concerned about this for two reasons: first, there will almost never be a scenario in which we want to model the system dynamics when all detunings are zero and second, the rest of the model-generated plots are in very strong agreement with the published plots from Nguyen and Tsai in both location and relative amplitudes of the peaks. So, we considered our results from this section to be a second verification of our model.

4.1.3 Verification of Set 3

Set 3 consists of two plots which are very similar to those in Set 2, except the pump and coupling Rabi frequencies are set equal to each other. In other words, the plots in Set 3 illustrate the relationship between the FWM signal intensity and Δ_p/Γ_2 for various values of Ω_p and Ω_c. The results published by [Nguyen and Tsai] demonstrating this relationship are in Figure 4.9, with relevant system parameters listed in Table 4.3.

Parameter	Value of Parameter for (a), in 2π MHz	Value of Parameter for (b), in 2π MHz
Δ_p	varied	varied
Δ_c	0	0
Δ_d	0	0
Ω_p	$0.01\Gamma_2$	$0.01\Gamma_2$
Ω_c	Ω_d	Ω_d
Ω_d	see legends	see legends
Γ_2	6.1	6.1
Γ_3	0.61	4.9
Γ_4	6.1	6.1

Table 4.3: System parameters used by [3] to plot Figure 4.9, which we used to verify our model.

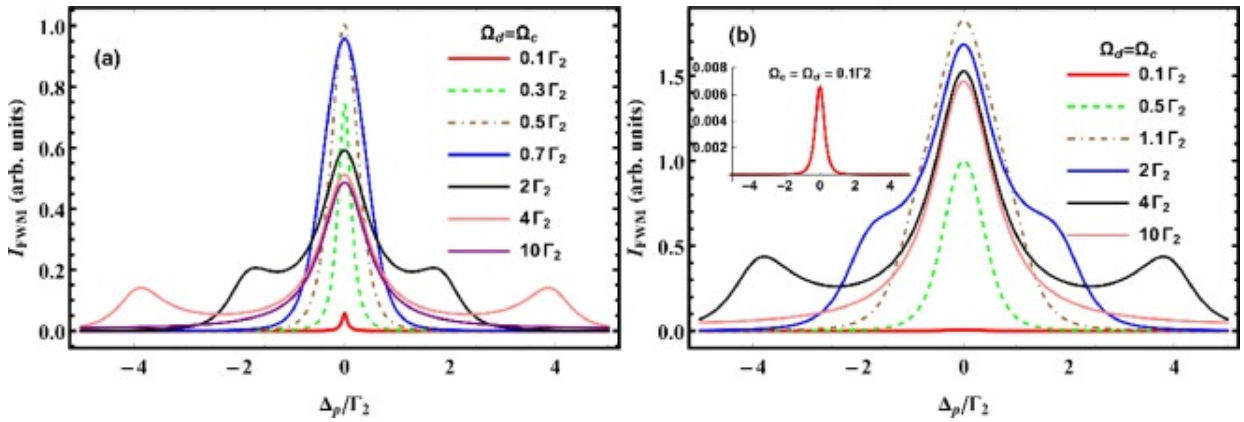

Figure 4.9: As Figures 5(a) and 5(b) from [3], these are the published plots of FWM signal intensity as a function of Δ_p/Γ_2. For each plot, $\Omega_c = \Omega_d$, and each curve corresponds to that generated by the system with a given value of these detunings, shown in the legend on the right of the frame. To see the relevant system parameters, see Table 4.3.

For comparison, the plots generated by our model using the same system parameters (Table 4.3) are shown in Figures 4.10 and 4.11. Oncemore, we see very strong agreement

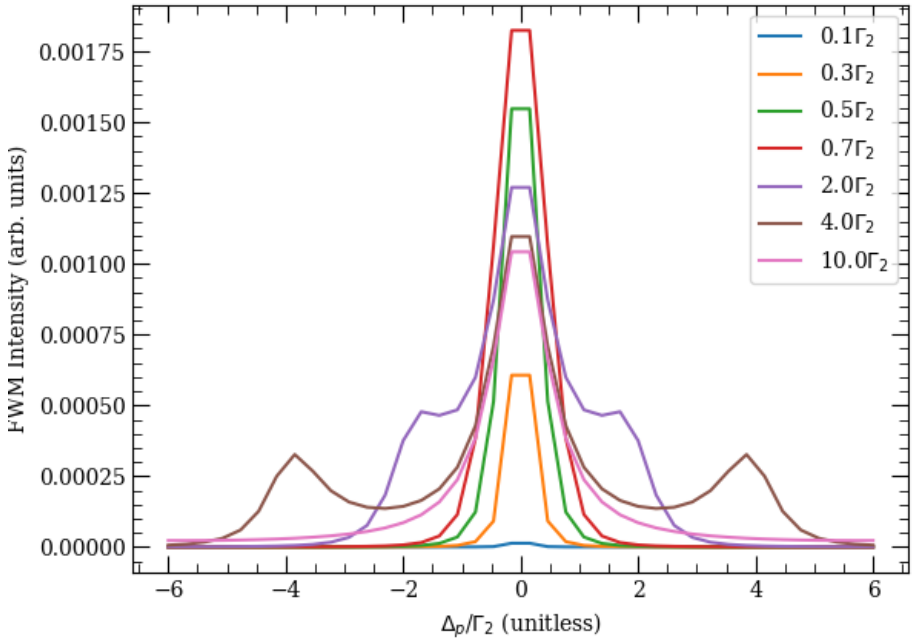

Figure 4.10: Plot of FWM signal intensity against Δ_p/Γ_2 with $\Omega_c = \Omega_d$ shown in the legend on the right, produced by our model. This corresponds to (a) in Figure 4.9. To see all relevant system parameters, see Table 4.3.

between the published and model-generated results, both in terms of where the peaks are located and their relative amplitudes. Similar to the model-generated plots in Set 2, the peaks at $\Delta_p/\Gamma_2 = 0$ are not nicely rounded as they are in Nguyen and Tsai's results, but this is not concerning and again serves as a reminder that the model works best for systems with significant detuning of at least one frequency.

4.1.4 Comments on these Results

In general, we found the results from these tests to be a meaningful first step in the verification of our model, especially considering that the only points where there was a significant discrepancy between the model's results and those published by Nguyen and Tsai occurred at $\Delta_p/\Gamma_2 = 0$. However, because these plots can only tell us about the FWM signal intensity in terms of arbitrary units, more testing was needed to ensure that the model produced the quantitative results we'd expect.

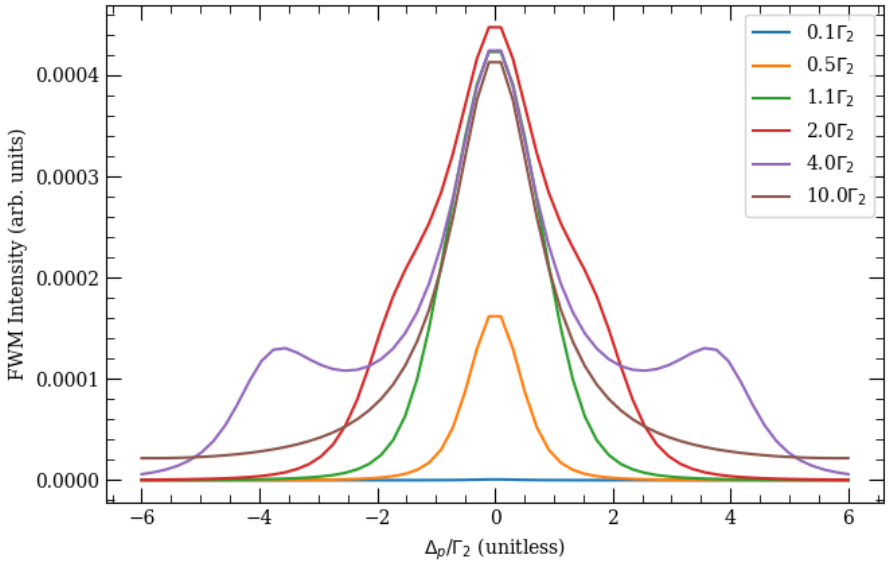

Figure 4.11: Plot of FWM signal intensity against Δ_p/Γ_2 with $\Omega_c = \Omega_d$ shown in the legend on the right, produced by our model. This corresponds to (a) in Figure 4.9. To see all relevant system parameters, see Table 4.3.

4.2 Verification with Quantitative Methods

The agreement of our model and Nguyen and Tsai's plots reassured us that the model was at least somewhat correct, but the confidence we could have in it based on these results alone was quite limited. This is mainly because the proportionality approach can only tell us about the FWM process up to arbitrary units. In other words, it allows us to see the relative magnitudes of the FWM signals as functions of different parameters, but it doesn't tell us anything too meaningful about the *actual* magnitudes that we're dealing with, which is not very helpful when the goal of the project was to calculate the FWM efficiency of a hypothetical system. So, we decided that the next logical step was to verify that the model's explicit efficiencies were consistent with those found via experiment, focusing primarily on confirming that the two sets of results would have the same order of magnitude.

Since we don't have experimental data of our own, we needed to find published results to use for our verification process. Unfortunately, there is very little data available for FWM stimulated in stationary trapped atoms, but there is a wide variety of experimental data available for FWM stimulated in warm atomic vapors [4, 5, 11]. Since we had used [11] to guide the construction of the model, we used its experimental results in a Rb-85 vapor to verify the model because we were particularly familiar with the system. We decided that

this data would be appropriate to use for verification, so long as we could find a way to "convert" the single-atom results to vapor cell results and vice-versa.

4.2.1 Experimental Results Used

To verify our model, we used the data from Figure 5 in [11], which plots the generated signal power against the power of the drive beam. Defining the FWM efficiency as

$$\epsilon_{FWM} = \frac{P_{signal}}{P_{drive}} \tag{4.1}$$

we can take the efficiency to be the slope of the plotted lines. Taking points from Willis et al.'s Figure 5, we have the following data points we can use to compare to our model:

Pump Power (mW)	Drive Power (μW)	Signal Power (nW)	FWM Efficiency
115	200	20	0.00010
50	1000	48	0.000048
15	1000	24	0.000024

Table 4.4: Experimental data from [Willis] used for model verification

There is a good amount of uncertainty in the Table 4.4 data because the intervals on the x- and y-axes of Willis' et al.'s Figure 5 are quite large with no intermediate markings to guide my estimations. Rather, the only tool to help me with that was a ruler. Despite this, we were content with using this data for our testing because our goal was to get the results from the model to agree with the published results within an order of magnitude, which is much larger than any potential uncertainty introduced by my limited estimations.

In addition to the pump and drive powers listed in Table 4.4, we used the following additional parameters from [11]:

- coupling power: 5 mW
- pump detuning: -1.5 GHz; coupling and drive beams on resonance
- beam waists: 1 mm for all beams
- FWHM of the atoms' velocity distribution: 2 m/s
- temperature of vapor: 100° C $\rightarrow$ T = 373 K
- beam geometry shown in Figure 4.12

Unfortunately, Willis et al. did not specify the detunings of the coupling and drive beams, so we set these to zero while testing our model. This is also a very likely source of uncertainty, but since our success criteria were so generous, we decided to postpone any concerns about this unless the results produced by the model didn't agree with the published ones.

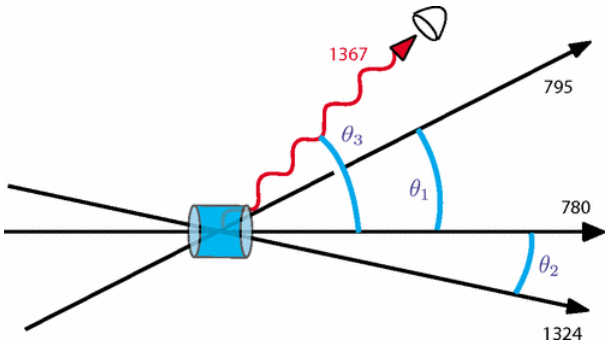

Figure 4.12: The beam geometry used in [11], which is relevant for calculating the volume of beam intersection using our model. Note that $\theta_1 = 2°$, $\theta_2 = 0.7°$, $\theta_3 = 2.7°$.

4.2.2 Converting Vapor Results to Single-Atom Results

As you might expect, results for FWM in a vapor cell and for trapped atoms or ions are not immediately comparable due to their differing velocity distributions. To account for this, we performed the following procedure.

First, we needed to determine the volume of the intersection of the beams in Willis et al.'s setup, which is required to determine in how many atoms FWM could potentially be stimulated, temporarily ignoring the velocity distribution. We modeled the volume enclosed by the intersection of the $1/e^2$ radii of the beams with a simple numerical integration script, which calculated the volume of intersection to be $V = 88.4 \cdot 10^{-9}\,\mathrm{m}^3$.

From here, it's necessary to determine how many atoms are contained in this intersection volume, which we'll call n_{tot}. Approximate the Rb-85 vapor to be an ideal gas, which is appropriate since the vapor pressure is quite low: the vapor pressure of Rb-85 at 100° C is $P = 266.6 \cdot 10^{-4}$ Pa. Then,

$$\begin{aligned} PV &= n_{tot} k_B T \\ n_{tot} &= \frac{PV}{k_B T} \\ &= 4.58 \cdot 10^{11} \end{aligned}$$

Due to Doppler shifting, only a fraction of the n_{tot} atoms in the volume of beam intersection will be able to participate in FWM. So, the next step is to calculate what that fraction is, which we'll call f_{part}. To do this, integrate the one-dimensional velocity distribution as we did in Equation 4.2. Notice that the limits of integration are -1 and 1, which we can find from centering the integral at 0, where the atoms are 'seen' as stationary by the incident beams, and integrating over the FWHM of the velocity distribution, which is 2 m/s.

$$\begin{aligned} f_{part} &= \frac{m_{Rb}}{k_B T\sqrt{2\pi}} \int_{-1\text{ m/s}}^{1\text{ m/s}} \exp\left(\frac{m_{Rb}v^2}{2k_B T}\right)\, dv \\ &= 0.00002 \end{aligned} \tag{4.2}$$

Then, the number of atoms participating in the process n_{part} is given by

$$\begin{aligned} n_{part} &= f_{part} \cdot n_{tot} \\ &= 1.0 \cdot 10^7 \end{aligned}$$

So, of the n_{tot} atoms in Willis, et al.'s Rb-85 vapor, only 10^7 are actually contributing to the FWM process. It follows that to convert our model's results, which are for single atoms, to Willis et al.'s for verification, we need to multiply the model's efficiency by 10^7 to appropriately scale to the number of participating atoms in the vapor.

4.2.3 Verifcation Using the Vapor Cell Results

Now that we know how to account for the relevant differences between the vapor cell and single-atom systems, we are ready to compare the model's efficiencies to Willis' experimental results. Table 4.5 shows the experimentally-determined FWM efficiencies from [11] juxtaposed with the results from our calculator.

Notice that with 115 mW of pump power, the experimental and calculated FWM efficiencies are in satisfactory agreement with each other. When 50 mW pump power is used, the experimental efficiency is $\frac{3}{2}$ times as large as the efficiency calculated by the model. The case with least agreement between experimental and calculated FWM efficiencies is that with 15 mW of pump power, in which the experimental FWM efficiency is 3 times larger than the FWM efficiency calculated by the model. I can think of circumstances in which this degree of disagreement would be concerning, however the main goal of this brief testing was to confirm that the model could agree with experimental data within an order of magnitude.

Pump Power (mW)	Experimental FWM Efficiency from [11]	FWM Efficiency from our model
115	0.00010	0.00010
50	0.000048	0.000032
15	0.000024	0.000008

Table 4.5: Experimental FWM Efficiencies from [11] compared to the FWM Efficiencies calculated by our model with the same parameters. Recall that to compare the efficiencies, the single-atom result from the calculator was multiplied by $n_{part} = 10^7$ to account for the fact that the published results involve 10^7 times as many participating atoms.

Since the largest factor of disagreement we found is 3, which is significantly lower than 10, we determined that the goal of the test was met, and we believe with a good amount of confidence that the model can accurately demonstrate both qualitative and quantitative relationships between system parameters such as laser detunings and laser powers and FWM efficiency.

4.3 Summary

We've verified our model using two methods, one for the proportionality approach and one for the explicit approach. There was strong agreement between the calculator and the results from [3] and satisfactory agreement between the model's results and those from [11], which we believe are sufficient to feel confident in the model's accuracy.

Chapter 5

Application to a Cesium System

In this section, I will present a brief application of the model to a trapped-cesium system and comment on how we might be able to most efficiently use it to determine if FWM-based measurement is viable.

5.1 Cesium System Modeled

The cesium system this section will model is a diamond-level structure where $|1\rangle$, $|2\rangle$, and $|4\rangle$ are chosen as described in Section 2.3 and $|3\rangle$ is chosen to be the $8S_{1/2}$ level such that the signal photon has a 752 nm wavelength.

Then, the laser wavelengths required are 852, 895, and 795 nm, the last of which is somewhat challenging to lock to the $|2\rangle > |3\rangle$ transition, but is possible using double-resonance optical pumping spectroscopy (DROP) techniques. The generated 752 nm signal is easily-filterable from the rest of these wavelengths, so this choice of system will work for the FWM measurement scheme, assuming that the efficiency is satisfactory, which we'll check in the following sections.

5.2 System Parameters

The cesium system we're modeling in this section is rather arbitrary in the sense that it's not based on a preexisting set of available hardware. As such, we don't have any system parameters to 'start' with, such as maximum laser powers or beam waists, and instead we are allowed the flexibility of choosing a setup. So, to make things a bit easier, we'll be using some of the system parameters from [11], such as the beam sizes and laser powers, but we'll apply these to a cesium atom rather than the rubidium-85 we used while verifying the model

in Chapter 4. It's very likely that this is not an ideal setup and that in future work with the model, the setup should be chosen differently.

The system parameters held constant for each test are in Table 5.1.

Parameter	Value of Parameter for Test 1	Value of Parameter for Test 2	Value of Parameter for Test 3
Δ_d	0 MHz	0 MHz	0 MHz
Pump Power	115 mW	50 mW	15 mW
Coupling Power	5 mW	5 mW	5 mW
Drive Power	200 μW	1000 μW	1000 μW
Γ_2	$32.8 \cdot 2\pi$ MHz	$32.8 \cdot 2\pi$ MHz	$32.8 \cdot 2\pi$ MHz
Γ_3	$11.1 \cdot 2\pi$ MHz	$11.1 \cdot 2\pi$ MHz	$11.1 \cdot 2\pi$ MHz
Γ_4	$28.7 \cdot 2\pi$ MHz	$28.7 \cdot 2\pi$ MHz	$28.7 \cdot 2\pi$ MHz
Beam Waists	0.001 m	0.001 m	0.001 m

Table 5.1: System parameters used to model our cesium system, with relevant laser powers taken from [11].

5.3 Results

In this section, we'll show the results of three tests, named Tests 1-3, mimicking the structure from Chapter 4: first, we'll plot the optical power of the FWM signal as a function of the coupling detuning to see for which values the FWM signal is maximized. Then, we'll set the coupling detuning to one of these values and repeat the process for the pump detuning, oncemore taking the value where the power of the FWM signal is maximized to create a pair of coupling and pump detunings that might yield a near-maximal FWM signal. Then, we'll calculate the FWM signal power for these chosen parameters just to see what kinds of generated powers are possible.

It's important to note that this optimization strategy is not ideal for a few reasons. First, assuming that optimal FWM results can be generated with the drive beam on-resonance is more for convenience than rooted in physics. Second, it would be best to attempt to optimize the output power of the FWM signal by adjusting the detunings simultaneously rather than separately, as we'll do in this section. Even if the detunings can be simultaneously optimized, the laser powers also require optimization, which adds to the complexity of the problem. Attempting to do a simultaneous parameter optimization with the current state of the model's code would be extremely computationally- and time-intensive. Developing an efficient optimization algorithm is likely a necessity for this model to be as useful as possible

but it is outside the scope of this thesis.

5.3.1 Test 1.

For this test, the pump power is 115 mW, the coupling power is 5 mW, and the drive power is 200 μW, which are parameters from [11].

Figure 5.1 plots of the FWM signal intensity in W against the coupling detuning Δ_c for the Test 1 parameters. From this plot, we can see that when $\Delta_p = \Delta_d = 0$, the FWM signal intensity is greatest when $\Delta_c \approx \pm 100 \cdot 2\pi$ MHz. Fixing Δ_c to $100 \cdot 2\pi$ MHz, the plot of FWM power while scanning the pump detuning Δ_p is shown in Figure 5.2. Although in Figure 5.1 there are maxima at both $\Delta_c = 100 \cdot 2\pi$ MHz and $\Delta_c = -100 \cdot 2\pi$ MHz, flipping the sign on the detuning only reflects the FWM power vs. Δ_p curve across $\Delta_p = 0$, so we will focus on making one plot with the positive Δ_c fixed.

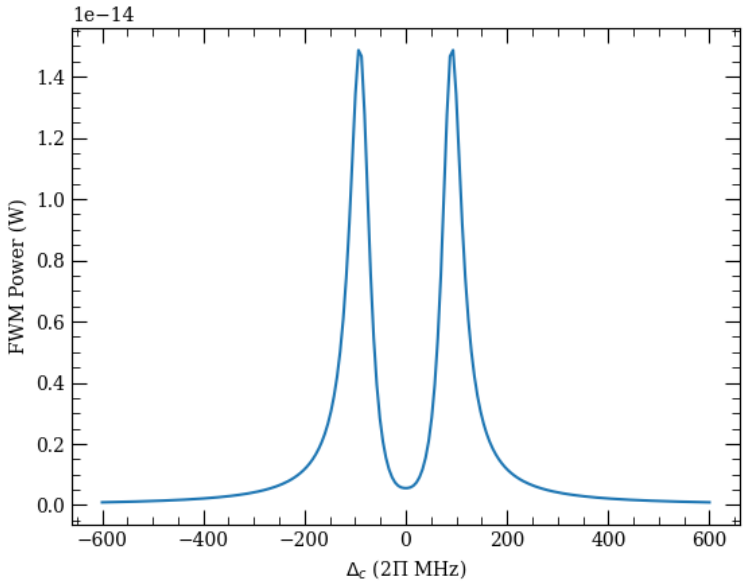

Figure 5.1: Plot of FWM signal power in W against the coupling detuning Δ_c with $\Delta_d = \Delta_p = 0$ and other Test 1 parameters in Table 5.1.

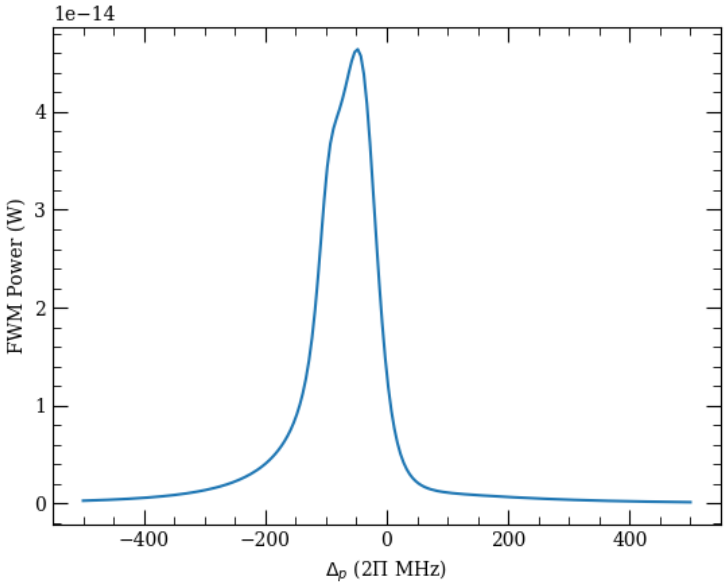

Figure 5.2: Plot of FWM signal power in W against the pump detuning Δ_p with $\Delta_d = 0$, $\Delta_c = 100 \cdot 2\pi$ MHz, and other Test 1 parameters in Table 5.1.

In Figure 5.2, it's clear that the FWM signal power is maximized when $\Delta_p \approx -50 \cdot 2\pi$ MHz, which we will fix for the next tests. We'll calculate the FWM efficiency and signal powers for a few sets of parameters with $\Delta_c = 100 \cdot 2\pi$ MHz and $\Delta_p = -50 \cdot 2\pi$ MHz, shown in Table 5.2. The efficiencies and output powers are in Table 5.3.

Parameter	Value of Parameter for Test 1.1	Value of Parameter for Test 1.2	Value of Parameter for Test 1.3
Δ_p	$-50 \cdot 2\pi$ MHz	$-50 \cdot 2\pi$ MHz	$-50 \cdot 2\pi$ MHz
Δ_c	$100 \cdot 2\pi$ MHz	$100 \cdot 2\pi$ MHz	$100 \cdot 2\pi$ MHz
Δ_d	0 MHz	0 MHz	0 MHz
Pump Power	115 mW	11.5 mW	1150 mW
Coupling Power	5 mW	0.5 mW	50 mW
Drive Power	200 μW	20 μW	2000 μW

Table 5.2: System parameters used to calculate FWM efficiencies and output powers, inspired by the parameters and results from Figures 5.1 and 5.2. The decay rates and beam waists are the same as in Table 5.1.

Result	Result for Test 1.1	Result for Test 1.2	Result for Test 1.3
FWM efficiency	$2.3 \cdot 10^{-16}$	$9.3 \cdot 10^{-17}$	$8.2 \cdot 10^{-19}$
FWM signal power	$4.6 \cdot 10^{-14}$ W	$1.9 \cdot 10^{-15}$ W	$1.6 \cdot 10^{-15}$ W

Table 5.3: FWM efficiencies and output powers, calculated using the system parameters from Table 5.2.

5.3.2 Test 2.

For this test, the pump power is 50 mW, the coupling power is 5 mW, and the drive power is 1000 μW, which are parameters from [11].

Figure 5.3 plots of the FWM signal intensity in W against the coupling detuning Δ_c for the Test 2 parameters. From this plot, we can see that when $\Delta_p = \Delta_d = 0$, the FWM signal intensity is greatest when $\Delta_c \approx \pm 55 \cdot 2\pi$ MHz. Fixing Δ_c to $55 \cdot 2\pi$ MHz, the plot of FWM power while scanning the pump detuning Δ_p is shown in Figure 5.4.

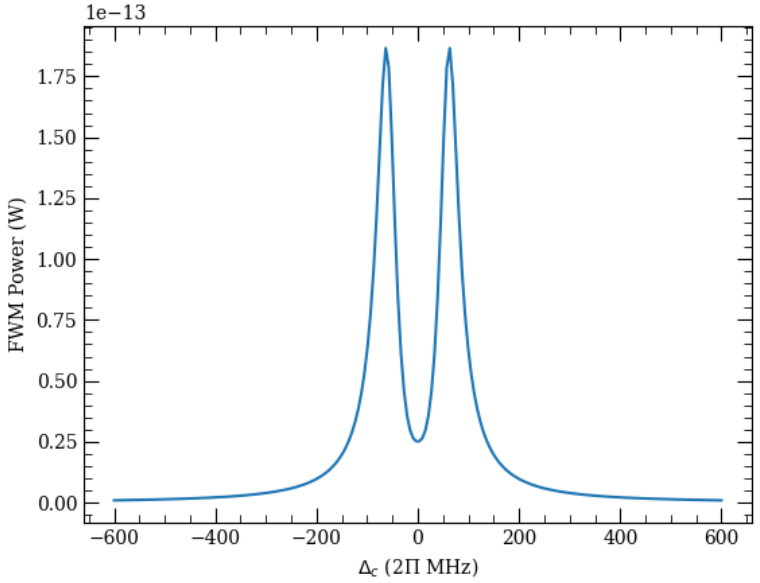

Figure 5.3: Plot of FWM signal power in W against the coupling detuning Δ_c with $\Delta_d = \Delta_p = 0$ and other Test 2 parameters in Table 5.1.

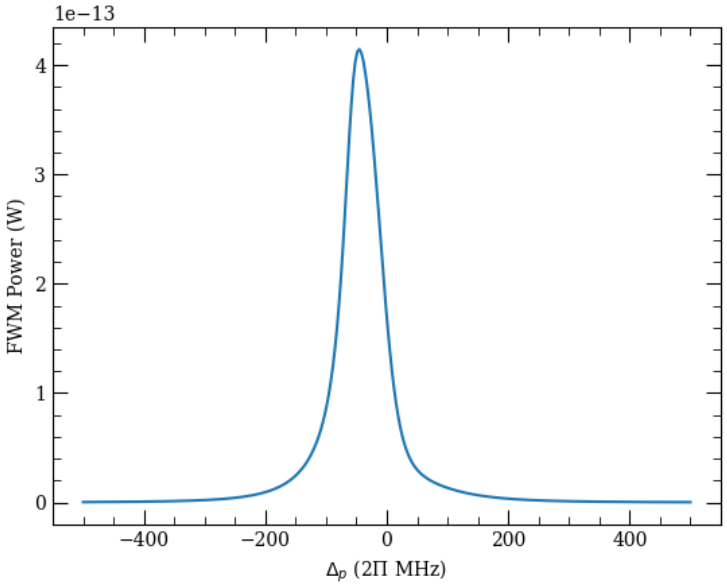

Figure 5.4: Plot of FWM signal power in W against the pump detuning Δ_p with $\Delta_d = 0$, $\Delta_c = 55 \cdot 2\pi$ MHz, and other Test 3 parameters in Table 5.1.

In Figure 5.4, it's clear that the FWM signal power is maximized when $\Delta_p \approx -50 \cdot 2\pi$ MHz, which we will fix for the next tests. Next, we'll calculate the FWM efficiency and signal powers for a few sets of parameters with $\Delta_c = 55 \cdot 2\pi$ MHz and $\Delta_p = -50 \cdot 2\pi$ MHz, shown in Table 5.4. The efficiencies and output powers are in Table 5.5.

Parameter	Value of Parameter for Test 2.1	Value of Parameter for Test 2.2	Value of Parameter for Test 2.3
Δ_p	$-50 \cdot 2\pi$ MHz	$-50 \cdot 2\pi$ MHz	$-50 \cdot 2\pi$ MHz
Δ_c	$55 \cdot 2\pi$ MHz	$55 \cdot 2\pi$ MHz	$55 \cdot 2\pi$ MHz
Δ_d	0 MHz	0 MHz	0 MHz
Pump Power	50 mW	5 mW	500 mW
Coupling Power	5 mW	0.5 mW	50 mW
Drive Power	1000 μW	100 μW	10000 μW

Table 5.4: System parameters used to calculate FWM efficiencies and output powers, inspired by the parameters and results from Figures 5.3 and 5.4. The decay rates and beam waists are the same as in Table 5.1.

Result	Result for Test 2.1	Result for Test 2.2	Result for Test 2.3
FWM efficiency	$4.1 \cdot 10^{-16}$	$8.7 \cdot 10^{-16}$	$6.7 \cdot 10^{-18}$
FWM signal power	$4.1 \cdot 10^{-13}$ W	$8.7 \cdot 10^{-14}$ W	$6.7 \cdot 10^{-14}$ W

Table 5.5: FWM efficiencies and output powers, calculated using the system parameters from Table 5.4.

5.3.3 Test 3.

For this test, the pump power is 15 mW, the coupling power is 5 mW, and the drive power is 1000 μW, which are parameters from [11].

Figure 5.5 plots of the FWM signal intensity in W against the coupling detuning Δ_c for the Test 3 parameters. From this plot, we can see that when $\Delta_p = \Delta_d = 0$, the FWM signal intensity is greatest when $\Delta_c \approx \pm 25$ MHz. Fixing Δ_c to 25 MHz, the plot of FWM power while scanning the pump detuning Δ_p is shown in Figure 5.6.

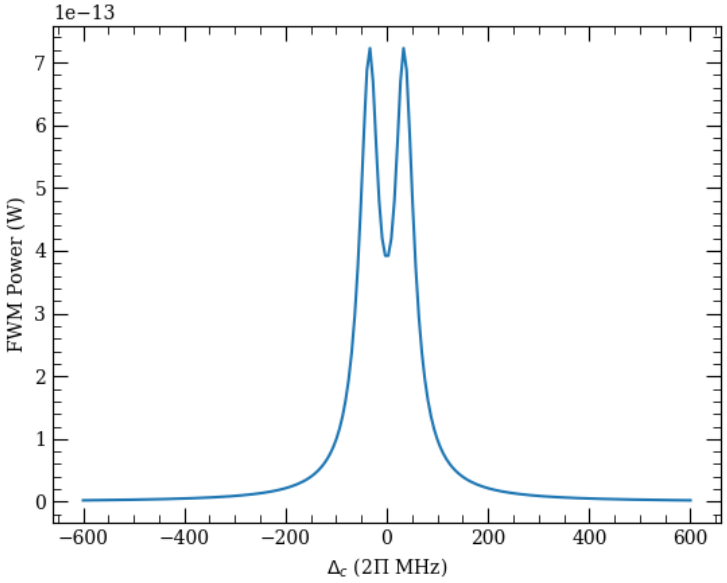

Figure 5.5: Plot of FWM signal power in W against the coupling detuning Δ_c with $\Delta_d = \Delta_p = 0$ and other Test 3 parameters in Table 5.1.

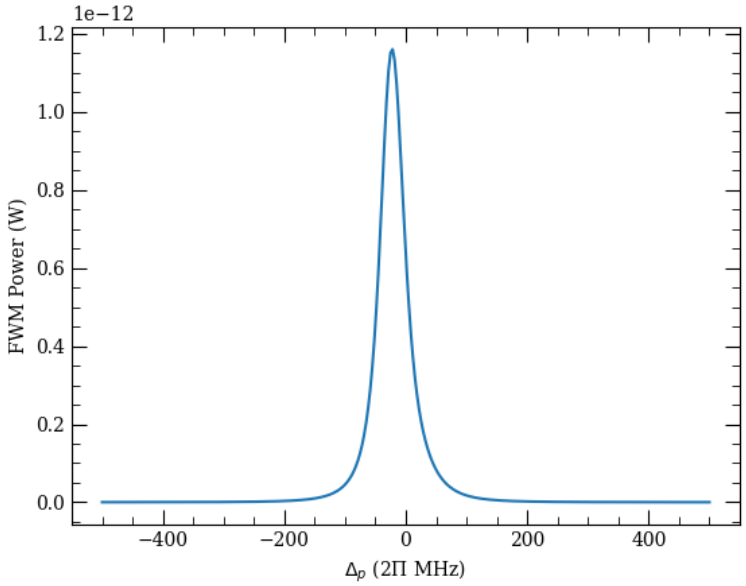

Figure 5.6: Plot of FWM signal power in W against the pump detuning Δ_p with $\Delta_d = 0$, $\Delta_c = 25$ MHz, and other Test 3 parameters in Table 5.1.

In Figure 5.6, it's clear that the FWM signal power is maximized when $\Delta_p \approx -25 \cdot 2\pi$ MHz, which we will fix for the next tests. We'll calculate the FWM efficiency and signal powers for a few sets of parameters with $\Delta_c = 25 \cdot 2\pi$ MHz and $\Delta_p = -25 \cdot 2\pi$ MHz, shown in Table 5.2. The efficiencies and output powers are in Table 5.3.

Parameter	Value of Parameter for Test 3.1	Value of Parameter for Test 3.2	Value of Parameter for Test 3.3
Δ_p	$-25 \cdot 2\pi$ MHz	$-25 \cdot 2\pi$ MHz	$-25 \cdot 2\pi$ MHz
Δ_c	$25 \cdot 2\pi$ MHz	$25 \cdot 2\pi$ MHz	$25 \cdot 2\pi$ MHz
Δ_d	0 MHz	0 MHz	0 MHz
Pump Power	15 mW	1.5 mW	150 mW
Coupling Power	5 mW	0.5 mW	50 mW
Drive Power	1000 μW	100 μW	10000 μW

Table 5.6: System parameters used to calculate FWM efficiencies and output powers, inspired by the parameters and results from Figures 5.5 and 5.6. The decay rates and beam waists are the same as in Table 5.1.

Result	Result for Test 3.1	Result for Test 3.2	Result for Test 3.3
FWM efficiency	$1.2 \cdot 10^{-15}$	$8.6 \cdot 10^{-16}$	$3.5 \cdot 10^{-17}$
FWM signal power	$1.15 \cdot 10^{-12}$ W	$8.6 \cdot 10^{-14}$ W	$3.5 \cdot 10^{-13}$ W

Table 5.7: FWM efficiencies and output powers, calculated using the system parameters from Table 5.6.

5.4 Comments

There are two overarching themes shared by the results of each test above that stand out the most: the first is that the generated signal power is very low, even for somewhat-high input laser powers such as in Tests 2.3 and 3.3. The generated signal powers the model calculated for single-atom FWM range from picowatts to femtowatts. These are extremely-low powers and are likely unusable with even the most cutting-edge photodetector or camera technologies. This is not a conclusion that FWM-based measurement wouldn't work, as the results could be poor because the parameters used for the tests were *completely* different than those that would produce a more satisfactory signal. This leads to the next stand-out theme, which is that these tests prove that a much more sophisticated testing protocol is required to truly optimize the FWM-based measurement scheme. It's also possible that the test system we made up would not produce good results even when the parameters are optimized, but a slightly-different system would, which is another area for study that we'll discuss briefly later.

To summarize the tests performed above, we first optimized FWM output power as a function of Δ_c with the pump and drive beams on-resonance, then fixed Δ_c where the maximum occurred. Next, with the drive beam on resonance and the coupling beam detuned by Δ_c, we did the same optimization procedure but with the independent variable being Δ_p. The Δ_p at which the maximum occurred became the value Δ_p was fixed at for the "quantitative" tests, which calculated the FWM efficiency and signal power with the chosen detunings and three sets of powers: those from the Chapter 4 testing, those larger than the Chapter 4 values by a factor of 10, and those smaller than the Chapter 4 values by a factor of 10.

From looking at the results shown up to this point, it's challenging to deduce a relationship between the system parameters and the FWM signal power, which implies that independently optimizing one parameter at a time and choosing some far-apart laser powers is not an efficient way to make conclusions about the viability of a FWM-based measurement scheme, as we hinted might be the case at the beginning of this chapter.

Instead, truly optimizing the FWM signal power would require some sort of algorithm that can systematically choose parameters and evaluate their effects quickly, which the current model is not able to do. This is especially complicated by the fact that QuTIP cannot produce a continuous map of ρ_{43}, but only a discrete one. Despite this, it's likely possible to design some algorithm to perform this task well so we can make useful conclusions about the viability of this measurement scheme.

Chapter 6

Next Steps

The previous chapter effectively demonstrated the limits of our current model, so this section will outline some next steps that can be taken to improve the model's utility and to further explore FWM-based measurement schemes in more depth.

Modeling a 'Real' System

Something that made the tests in Chapter 5 significantly more challenging was that we did them without a specific physical system in mind. In other words, we didn't have much knowledge about the limitations that were put on our model by the lasers we wanted to use, etc. Instead, we just used parameters from [11], which didn't give us enough information about the lasers' maximum powers or how far they could be reliably detuned, or even how well we could manipulate the beam to improve the intensities used in the calculations. If the tests from Chapter 5 were re-done using a specific collection of lasers, we would have some guidance in terms of how 'far' we can change each parameter to get a useful conclusion from the model for a particular system.

One of the most obvious places to start with modeling a 'real system' is to switch to modeling a system with beam waists more similar to those used in true trapped-atom quantum information systems. One of the most glaring discrepancies between the test system from Chapter 5 and a 'real-life' trapped-atom qubit system is that a trapped-atom quantum computer will likely have beam waists on the order of a micron. Since the model relies heavily on intensity values (which are inversely proportional to the area spanned by the beam) to produce its results, reducing the beam waists by a factor of 10^3 should significantly impact the results the model returns.

Writing an Optimization Algorithm

As mentioned in the previous chapter, it's extremely difficult to make conclusions about the viability of a FWM-based measurement scheme without a systematic, efficient optimization algorithm that can determine which system parameters, if any, can yield a workable signal. This is likely the best place to start to improve the model but it's also the most challenging improvement to attempt since a poorly-written algorithm would take an exceptionally long time to compile. Factoring the system limitations described in the first suggestion into the algorithm would likely decrease its compile time, so these first two suggestions go hand-in-hand if you want to pursue the algorithmic approach to making conclusions about FWM-based readout schemes.

Making the Model More Physically Robust

This physics of this model are quite simplified. The cesium energy level diagrams shown in Chapter 2 indicate that the four-level system we've chosen to model in cesium doesn't really exist: rather, each of the levels in the system has hyperfine splittings, which could cause experiment to stray from the model. One of the most significant issues with this four-level approximation is that it cannot model what might happen if the system suffers a decoherence event where the electron doesn't decay to the state that the model assumes it would. For example, if we tune the lasers to address the $|1\rangle$ qubit state and set up the model to match, it's possible that throughout the process the electron decays to the $|0\rangle$ state, which is not included in the model as it assumes that the system has only four levels. In this case, the physical system would act entirely differently than what the model predicted: in experiment, the electron would be "lost", unable to be addressed by the lasers, but in the model, it would continue to participate in the FWM process. In this scenario, the model wouldn't give us a very clear idea about how well a FWM-based measurement scheme would work in practice.

So, it's likely a good idea to make the model more physically accurate by incorporating the hyperfine sublevels and the possible decay paths associated with their inclusion in order to better plan for and model these decoherence events and more accurately describe the dynamics of the system.

Chapter 7

Conclusion

This thesis sought to model the dynamics of a trapped atom involved in a FWM process, which could be used to determine if a FWM-based measurement scheme for trapped-atom qubits is viable. To work towards this goal, we derived expressions for the efficiency of the FWM process stimulated in an atom and the optical power of the generated signal, which were in satisfactory agreement with published results when tested against them. In addition to the generated expressions, we produced a model of the quantum dynamics of the relevant four-level system, which can give us even more insight into the FWM process such as how scanning various parameters affects its efficiency. The results produced by this model also have satisfactory agreement with published results, further increasing our confidence in our work.

The model and derived expressions offer a place to start to work towards making a conclusion about the viability of a FWM-based measurement scheme for trapped-atom qubits. It's important to recognize that without modeling a real hardware system and without doing more robust parameter optimization that that we are not in a good position to comment on the viability of FWM as a measurement scheme.

To work towards a model that can help to make a real decision on the viability of a FWM-based readout scheme, one can write the aforementioned efficient optimization algorithm, make the model more physically accurate, and test it with respect to an actual set of hardware components, which allows for the placement of limits on system parameters such as laser powers. Despite these opportunities for improvement, we're confident that this model is the first step towards a thorough analysis of this proposal for an alternative to measurement by resonance-fluorescence.

Bibliography

[1]D. A. Steck, *Cesium D Line Data*, 1998.

[2]A. G. Radnaev, "Towards quantum telecommunication and a Thorium nuclear clock", PhD thesis (Georgia Institute of Technology, Aug. 17, 2012).

[3]T.-T. Nguyen and C.-C. Tsai, "Four-wave mixing involving V type system: In view of dressed state picture", Chinese Journal of Physics **77**, 319–326 (2022).

[4]J. Wu, M. Guo, H. Zhou, J. Liu, J. Li, and J. Zhang, "Experimental realization of efficient nondegenerate four-wave mixing in cesium atoms", Opt. Express **30**, 12576 (2022).

[5]J. Hwang, J. Park, H. Kim, and H. S. Moon, "Stimulated four-wave mixing in the cascade-type atomic system of a warm Cs atomic ensemble", Opt. Express, OE **28**, Publisher: Optica Publishing Group, 35927–35936 (2020).

[6]D. J. Griffiths and D. F. Schroeter, *Introduction to Quantum Mechanics*, 3rd ed. (Cambridge University Press, 2018).

[7]D. Manzano, "A short introduction to the Lindblad master equation", AIP Advances **10**, 025106 (2020).

[8]*Lindblad Master Equation Solver*, QuTiP 4.7 Documentation, (Dec. 12, 2022) `https://qutip.org/docs/latest/guide/dynamics/dynamics-master.html` (visited on 04/03/2023).

[9]M. Parniak and W. Wasilewski, "Interference and nonlinear properties of four-wave-mixing resonances in thermal vapor: Analytical results and experimental verification", Phys. Rev. A **91**, 023418 (2015).

[10]E. A. Copenhaver, "Tune-out measurement in lukewarm lithium with phase-patterned atom interferometry", PhD thesis (University of California Berkeley, 2019).

[11]R. T. Willis, F. E. Becerra, L. A. Orozco, and S. L. Rolston, "Four-wave mixing in the diamond configuration in an atomic vapor", Phys. Rev. A **79**, 033814 (2009).

[12]D. J. Griffiths, *Introduction to Electrodynamics*, 4th ed. (Cambridge University Press, 2017).